의학박사 학위논문

Tumor angiogenesis imaging using cyclic RGD-PEGylated gold nanoparticles labeled with radioiodine

방사성 옥소 표지 cRGD-PEG 금 나노 입자를 이용한 종양 신생혈관 영상

2013 년 08 월

서울대학교 대학원
의과학과 의과학전공

김 영 화

A thesis of the Degree of Doctor of Philosophy

방사성 옥소 표지 cRGD-PEG 금 나노 입자를 이용한 종양 신생혈관 영상

Tumor angiogenesis imaging using cyclic RGD-PEGylated gold nanoparticles labeled with radioiodine

August 2013

The Department of Biomedical Sciences,
Seoul National University
College of Medicine

Young-Hwa Kim

방사성 옥소 표지 cRGD-PEG 금 나노 입자를 이용한 종양 신생혈관 영상

지도교수 정 준 기

이 논문을 의학 박사 학위논문으로 제출함
2013년 8월

서울대학교 대학원
의과학과 의과학전공
김 영 화

김 영 화의 의학박사 학위 논문을 인준함
2013년 8월

위 원 장 _____
부위원장 _____
위 원 _____
위 원 _____
위 원 _____

Tumor angiogenesis imaging using cyclic RGD-PEGylated gold nanoparticles labeled with radioiodine

by
Young-Hwa Kim

A thesis submitted to the Department of Biomedical Sciences
in partial fulfillment of the requirements
for the Degree of Doctor of Philosophy in Biomedical Sciences
at Seoul National University College of Medicine

August 2013

Approved by Thesis Committee:

Professor _____ **Chairman**
Professor _____ **Vice chairman**
Professor _____
Professor _____
Professor _____

ABSTRACT

Young-Hwa Kim
Department of Biomedical Sciences
The Graduate School
Seoul National University

Introduction: The biocompatibility of nanoparticles is important in biomedical field such as *in vivo* molecular imaging and drug delivery. To visualize the tumor angiogenesis, I developed ^{125}I-labeled gold nanoparticles (AuNPs) conjugated with cyclic RGD-PEG peptides.

Methods: I developed that cyclic RGD-PEGylated-AuNPs was labeled with ^{125}I (^{125}I-cRP-AuNPs) as molecular imaging probes for targeting integrin $\alpha_v\beta_3$. The stability of ^{125}I-cRP-AuNPs was monitored by ITLC-SG with saline (pH 7) as the solvent for 16 hrs at 37^{o}C in serum. For the competitive binding assay to the integrin $\alpha_v\beta_3$, ^{125}I-echistatin was incubated with $\alpha_v\beta_3$-expressing cancer cell, U87MG and non-expressing cancer cell, MCF7 after pre-treating with cRP-AuNPs or cRGD peptides. Cellular uptakes of ^{125}I were measured using gamma-counter. To confirm receptor specific internalization of cRP-AuNPs, TEM image was acquired in U87MG and MCF7 cell lines. The uptake and clearance of ^{125}I-cRP-AuNPs *in vivo* was evaluated using serial SPECT/CT studies from 0 hr to 5 hrs after intravenous injection of 11.1 MBq ^{125}I-cRP-AuNPs in a U87MG tumor bearing mice. To confirm specific

integrin $\alpha_v\beta_3$ binding of ^{125}I-cRP-AuNPs, the extracted tumor tissues were analyzed by TEM imaging technique and stained with $\alpha_v\beta_3$ integrin antibody. Renal clearance of ^{125}I-cRP-AuNPs was confirmed with radio-TLC analysis of urine samples after injection.

Results: The entire ^{125}I labeling procedure to cyclic RGD-PEGylated gold nanoparticles was completed within 20 min including purification and concentration steps. Radio-chemical purity of ^{125}I-labeled cRGD-AuNPs was very stable during the incubation in serum at 37^{o}C. In competitive binding assay to U87MG cells, IC_{50} values for cRP-AuNPs and cRGD peptides were 0.33 nM and 51.34 nM, respectively. Remarkably, the ^{125}I-cRP-AuNP probes showed ~150-fold higher $\alpha_v\beta_3$ avidity than the corresponding cRGD peptides. TEM images showed intracellular localization of the particles in U87MG cells only, not in MCF7 cells. SPECT/CT image showed uptakes of ^{125}I-cRP-AuNPs in the U87MG xenografted tumor and blood pool until 1 hr after injection. In the extracted tumor analysis, the TEM images clearly showed the ^{125}I-cRP-AuNPs are uptake by the tumor. And the tumor tissue was well correlated with $\alpha_v\beta_3$-PE staining regions and Au silver enhancement. These results demonstrate that the ^{125}I-cRP-AuNPs entered the tumor via integrin $\alpha_v\beta_3$-receptor specific endocytosis. Radio-chemical yield of urine samples was observed over 50% of ^{125}I-cRP-AuNPs, this result showed their efficient

clearance from the body through renal and urinary excretion route.

Conclusion: ^{125}I-cRP-AuNPs defined $\alpha_v\beta_3$ expressing cancer cells both *in vitro* and *in vivo*. These functionalized ^{125}I-cRP-AuNPs have a visualization in tumor and angiogenesis which will be useful for various diagnostic and therapeutic applications.

Keywords: gold nanoparticles, nanoparticle toxicity, tumor angiogenesis targeting, tumor angiogenesis imaging, integrin $\alpha_v\beta_3$, iodine-125, SPECT/CT

Student number: 2008-23291

CONTENTS

LIST OF FIGURES AND TABLES

LIST OF ABBREVIATIONS

AuNPs, Colloidal gold nanoparticles

PEG, Poly (Ethylene Glycol)

RGD, cRGDyK, cyclic Arg-Gly-Asp-D-Tyr-Lys

cRP-AuNPs, cyclic RGD-PEGylated AuNPs

TEM, Transmission Electron Microscopy

DLS, Dynamic Light Scattering

RT-PCR, Reverse Transcription-Polymerase Chain Reaction

SDS, Sodium Dodecyl Sulfate

FBS, Fetal Bovine Serum

HBSS, Hank's Balanced Salt Solution

^{125}**I,** Iodine-125

SPECT/CT, Single Photon Emission Computed Tomography/Computed Tomography

%ID/g, % Injected Dose/gram

ITLC-SG, Instant Thin Layer Chromatography-Silica Gel

GAA, GlutArAldehyde

INTRODUCTION

1. *In vivo* molecular imaging and its application

In vivo molecular imaging such as MRI, positron emission tomography (PET) plays a crucial role in diagnosis and therapy of diseases and understanding of biological processes (*1-4*). Recently, molecular imaging is widening its fields through revealing molecular events in cells and tissues (5-*7*). Molecular imaging is useful not only for clinical studies but also for developing new drugs and new treatment modalities such as gene or stem cell therapy (*8*,9). Pre-clinical molecular imaging using animals such as mice shows biodistribution, pharmacokinetics, mechanism of action, and efficacy *(10)*. And also newly developed various materials for biomedical application fields can be validated using molecular imaging methods (*11-13*). For imaging modalities with low sensitivity, nanoparticles bearing multiple contrast groups provide signal amplification. The same nanoparticles can deliver both contrast medium and drug, allowing monitoring of biodistribution and therapeutic activity simultaneously. So, Collaboration among biomedical researchers, materials scientists, and device engineers is prerequisite.

2. Nanomaterials for biomedical application

Nanomaterials are amorphous or semi-crystalline structures with at least one dimension ranging between 10 and 100 nm. Several of their characteristics, such as size uniformity, surface area, adsorption kinetics, biocompatibility, can be finely tuned during the production process for specific purposes (*14,15*). Nanomaterials offer several advantages as therapeutic and diagnostic tools due to various sizes, large surface area, and ease of surface modification with multivalent ligands from biological components such as various peptides, antibodies, fluorescent dye, radioisotope, drugs, genes, and targeting biomarkers (*16*). Recently, various types of nanoparticles have received great interest for molecular imaging because of their advantageous properties including multifunctionality and multivalency effects (*17-23*). Most biomedical nanomaterials require high specificity and sensitivity, which are typically achieved by conjugation of targeting ligands or imaging agents, for improved affinity (avidity) and targeting efficiency (*24-26*).

Colloidal gold nanoparticles (AuNPs) are an attractive candidate as imaging probes because these particles show little or no cytotoxicity in

various cells and animal models (*27-31*). Moreover, AuNPs can be easily modified with biomolecules (e.g., DNA and peptides) via thiol-Au bonds, and many other functional ligands can also be incorporated simultaneously. Another merit for these particles is that anti-biofouling polymers such as polyethylene glycol (PEG) can be readily loaded on AuNP surfaces for the preparation of highly stable and specific probes as well as efficient conjugation of targeting ligands (*32-35*).

As the imaging contrast agents, gold nanoparticles have been tried in various imaging modalities. The use of AuNPs for optical imaging was restricted to superficial region due to the weak penetrating depth of visible light (*36,37*). X-ray-based computed tomography (CT) suffered from low detection sensitivity of AuNPs, which results in a requirement of high probe concentration (>100 mg/mL) (*38*). In the case of MRI using AuNPs, the surface modification of AuNPs is limited because most surfaces need to be covered by chelating units (chelating agents-gadolinium ions) for maximizing MR signal. This results in small surface areas left for the introduction of targeting molecules on AuNPs (*36*). Such insufficient penetration depth,

insensitivity or limited surface chemistry makes it difficult for *in vivo* monitoring.

In addition, iodine ion is known to have high affinity to gold atom, and these ions can be readily conjugated to AuNPs to form Au-I bonds on gold surfaces (*39-41*). Such a simple chemistry between iodine and AuNPs allow straightforward and efficient labeling of radioiodine to AuNPs without iodination reagents or iodine accepting functional groups such as a phenol residue. ^{125}I ($t_{1/2}$ = 60.14 days) is a commercially available low-energy gamma emitter with a long physical half-life, compared to other radioactive isotopes, and it can therefore be used for long-term monitoring (*42*). Therefore, nuclear medicine imaging using radioiodine can be considered good sensitivity and sufficient penetration depth to clinical applications of AuNPs.

3. Angiogenesis imaging for biomedical application

Angiogenesis imaging may turn out to have significant benefits because they evaluate other diseases characterized by abnormal angiogenesis, such as ischemic region and benign tumors. Already many research groups have shown the various radio-labeled RGD sequence targeted imaging method in biomedical area (*43-45*). However, a small peptide that consists of

the radio-labeled RGD sequence is quickly the washing out in vivo (*44*). Further, a long-blood half-life of nanoparticles is necessary for in vivo imaging and monitoring applications, and controlling the excretion of nanoparticles from human bodies is keys to the widespread use of non-degradable metallic nanoparticles for *in vivo* applications.

4. The aim of this study

To develop an *in vivo* monitoring probes targeting integrin $\alpha_v\beta_3$ in tumor angiogenesis, I evaluated the versatile carrier system with ^{125}I-labeled gold nanoparticles (AuNPs) conjugated with PEG-RGD peptides for targeting tumor.

MATERIAL AND METHODS

1. General remarks and materials

All commercially available chemical reagents were used without further purification. Gold(III) chloride trihydrate ($HAuCl_4.3H_2O$, 99.9+%) and Tween 20 were purchased from Sigma-Aldrich (St. Louis, MO, USA). Sodium citrate ($HOC(COONa)(CH_2COONa)_2.2H_2O$) was purchased from Sigma-Aldrich (St. Louis, MO, USA). Amine-PEG-thiol (MW 5000, NPS) was purchased from Laysan Bio, Inc. (Arab, AL, USA). Succinimidyl 4-[N-maleimidomethyl]cyclohexane-1-carboxylate (Sulfo-SMCC) was purchased from Thermo Scientific (Palm Springs, CA, USA). Cyclo (Arg-Gly-Asp-D-Tyr-Cys) (cRGD) was purchased from Peptides International (Louisville, KY, USA). $Na^{125}I$, [^{125}I] – Echistatin were obtained from Perkin Elmer Life Science, Inc. (Boston, MA, USA). ITLC-silica gel [SG] was purchased from Pal Gelman Laboratory (Pall Life Sciences, Ann Arbor, MI, USA). HQ silver enhancement kit was purchased from Nanoprobes Inc (Nanoprobes Inc. Stony Brook, NY, USA). Radiochemical purity was tested with AR-2000 radio-TLC scanner (Bioscan, Washington, DC, USA), A Cobra II γ-scintillation counter (Packard, Meriden, CT, USA) was used for the detection of radioactivity. Milli-Q water was used at every stage of reaction and washing. All phosphate-buffer solutions used were 10 mM unless noted. Fluorescence imaging was performed using a fluorescence microscope (IX-71 Provis, Olympus, Rungis, France). A small-animal image was used for SPECT/CT scanner (Bioscan, Washington DC, WA, USA).

2. Preparation of gold nanoparticles

2.1 Synthesis of 13 nm gold nanoparticles.

13-nm gold nanoparticles (AuNPs) were synthesized, as described previously (Turkevich, J.; Hillier, J.; Stevenson, P. C. Discuss. Faraday Soc. 11, 55, 1951), by reducing a well-stirred solution of 100 mL of 1 mM chloroauric acid with 10 mL of 38.8 mM sodium citrate in deionized water under reflux. The solution was stirred for several hours to allow full reduction. Red-wine colored solution was cooled down to the room temperature. The particle concentration was estimated at ~ 10 nM, with extinction coefficient of 2.8×10^8 at the peak 520 nM, 1 cm path length. The solution was kept at 4^oC and in dark condition.

2.2 Preparation of amine-PEG-thiol modified gold nanoparticles

To prepare PEGlyated Gold Nanoparticles, AuNPs were first treated with Tween 20. A 500 μL amount of 1 mM Tween 20 was added to 5 mL of 13 nm AuNPs and the mixture was stirred for 10 min. After addition of 1 mL Amine-PEG-Thiol (MW 5000, NPS, 2500 equiv.), the mixture was stirred for 3 h to allow complete exchange of the citrate with thiol. The mixture was then purified by centrifugation (15000 rpm for 30 min at 4^oC) twice. The supernatant was removed, and the pellet was dispersed in 5 mL PB (pH 8.4).

2.3 Preparation of sulfo-SMCC/PEG-modified gold nanoparticles

The amine part of PEG on AuNPs was linked with Sulfo-SMCC which is a linker for cRGD peptide. To 1 mL of previously prepared PEGlyated AuNPs in PB, freshly made 100 μL of Sulfo-SMCC (400 μM) in PB (pH 8.4) was added. The mixture was vortexed for 1 hr and then purified by centrifugation (15000 rpm for 30 min at 4^{o}C) twice. The supernatant was removed, and the pellet was used in the following step.

2.4 Preparation of cRGD/Sulfo-SMCC/PEG-modified gold nanoparticles

To prepare cRGD-modified AuNPs, the pellet obtained from the previous step was redispersed in 100 μL of Cyclic RGD peptide (100 μM) in PB (pH 7.4) and the mixture was vortexed for 1 hr. It was then purified by a series of centrifugation (15000 rpm for 30 min each at 4^{o}C). The supernatant was removed, the pellet, obtained as a final product, was kept at 4^{o}C and in dark condition.

3.5 cRGD-PEGylated gold nanoparticles with ^{125}I radiolabeling

To prepare ^{125}I labeled AuNPs, 10 μCi/10 μL of [^{125}I]NaI in PBS solution was added to 100 μL cRP-AuNPs solution (7 nM), and the resulting solution was stirred for 5 min at room temperature. After the iodine-labeled cRGD-PEG-AuNPs (^{125}I-cRP-AuNPs) were purified by centrifugation (12000

rpm for 15 min). Radio-labeling efficiencies were monitored by ITLC-SG with saline (pH 7) as the solvent.

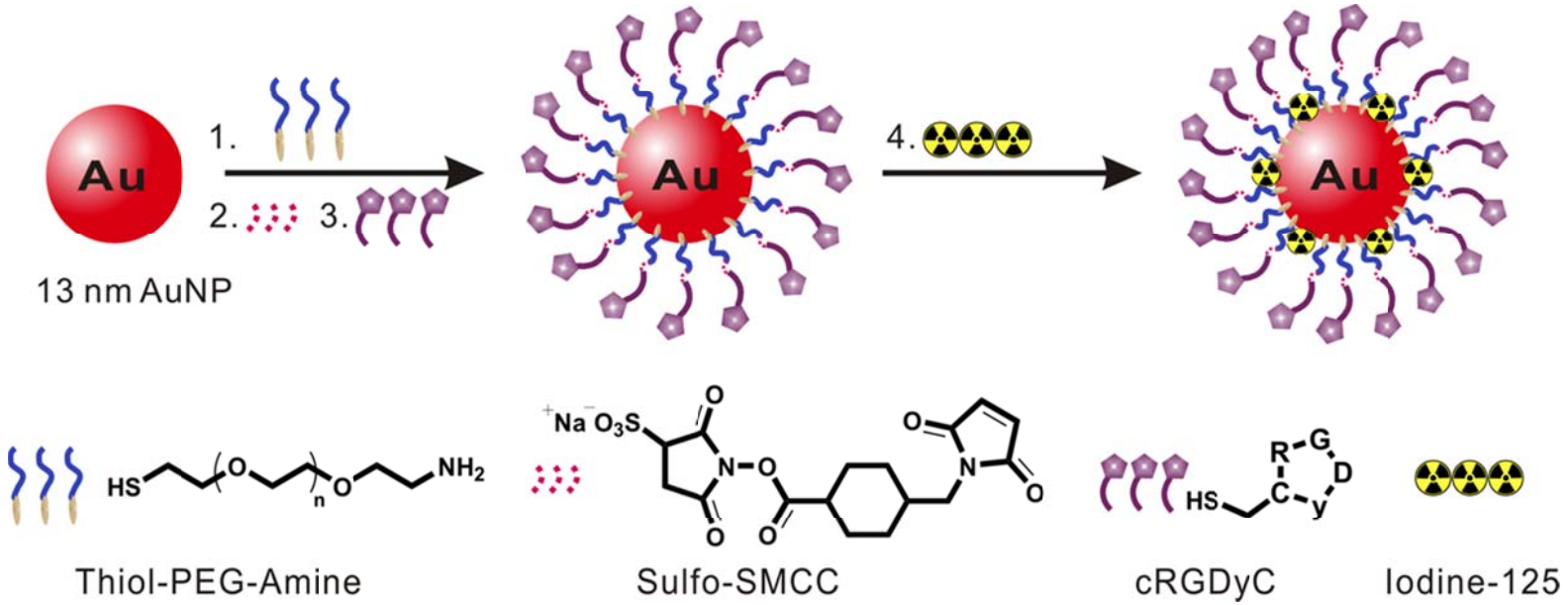
Au
1.
2.
3.
13 nm AuNP
Au
4.
Au
HS
O
n
O
NH2
Thiol-PEG-Amine
+Na −O3S
O
N
O
O
O
N
O
O
Sulfo-SMCC
HS
R
G
D
C
y
cRGDyC
Iodine-125

2.6 Sample characterization

Hydrodynamic diameter and size distributions of the purified encapsulated AuNPs were measured using dynamic light scattering (DLS, Malvern Zetasizer Nano ZS90 system, Malvern Instrument Ltd., England) and transmission electron microscopy (TEM, JEM-1400, JEOL, Tokyo, Japan). For DLS measurement, AuNPs solution was diluted 10 times in distilled water and mixed for 1 min by sonication. The particle size and distribution were obtained from the volume-percent (%) value at 25°C and at a scattering angle of 90°. To take negative-stain TEM images of encapsulated AuNPs, the solution was dropped on a Formvar-carbon coated copper grid and stained with saturated uranyl acetate solution. TEM images were taken using JEOL TEM with an acceleration voltage of 80 keV.

2.7 *In vitro* serum stability

The serum stability of ^{125}I-cRGD-AuNPs and ^{125}I-mPEG-AuNPs was tested by incubating ^{125}I-cRGD-AuNPs and ^{125}I-mPEG-AuNPs in fetal bovine serum (FBS) for 30 hrs at 37^{o}C to test in vitro serum stability. Radio-labeling efficiencies were monitored by ITLC-SG with saline (pH 7) as the solvent.

3. Cell culture and animals

Human malignant glioma U87MG cell line and human breast carcinoma MCF7 cell line were obtained from American Type Culture Collection (ATCC) and cultured in Minimum Essential Medium (MEM) and

Dulbecco's Modified Eagle Medium (DMEM) with 10% fetal bovine serum, 100 U/mL penicillin and 100 μg/mL streptomycin at 37°C in a humidified atmosphere containing 5% CO_2. Specific pathogen-free 6 - 7 weeks old BALB/c nude mice were obtained from Orient bio. (Korea). All the animal experiments were performed after receiving approval from the Institutional Animal Care and Use Committee (IACUC) of the Clinical Research Institute at Seoul National University Hospital.

3.1 *In vitro* study

3.1.1 RT-PCR analysis

The total RNA was isolated from U87MG and MCF7 cells using Trizol reagent (Invitrogen, Grand Island, NY, USA) according to manufacturer's instruction, and then reverse transcribed with a mixture of random hexamer primer, 5X RT buffer, DTT, and 50 U of M-MLV reverse transcriptase (Invitrogen, Grand Island, NY, USA). The sequences of the forward and reverse primers of α_v were 5'-GAAAAGAATGACACGGTTGC and 5'-TAACCAATGTGGAGTTGGTG, respectively. The sequences of the forward and reverse primers of β_3 were 5'-ACTGCCTGTGTGACTCCGACT and 5'-GGCTCTGGTGAGCAAGAAACA. The sequences of the forward and reverse primers of β-actin were 5'-ACCAGGGCTGCTTTTAACTCT and 5'-GAGTCCTTCCACGATACCAAA. The PCR reaction (94°C for 30 sec, 62°C or 60°C for 60 sec, 72°C for 2 min) was run for 30 cycles after an initial single cycle of 94°C for 10 min to activate the Taq polymerase, an additional

7 min at 72°C. And the annealing temperatures used for α_v and β_3 were 62°C, 60°C, respectively. After 30 cycles of amplification, PCR products were analyzed by gel electrophoresis in 1% agarose gels and visualized by Loading star (DyneBioInc, Seoul, Korea) staining.

3.1.2 Western blot analysis

Cells were lysed in radio-immunoprecipitation assay (RIPA) buffer (Sigma, St. Louis, MO, USA) containing protease inhibitor cocktail (Roche Diagnostics, Basel, Switzerland), and subsequently cleared via centrifugation. Protein concentrations were determined using BCA protein assay kit (Thermo Scientific, Palm Springs, CA, USA). Total protein (30 μg) mixed with 4X polyacrylamide gel electrophoresis sample buffer (Invitrogen, Grand Island, NY, USA) was separated via NuPAGE Novex 4 - 12% gradient Bis-Tris mini gels (Invitrogen, Grand Island, NY, USA) and transferred to nitrocellulose membranes. Membranes were blocked with 3% skim milk for 1 hr at room temperature, and then incubated with one of the following primary antibody overnight at 4°C anti-integrin $\alpha_v\beta_3$ (MAB3050, R&D Systems, Minneapolis, MN, USA; diluted 1:1000) or alpha-tubulin (Sigma, St. Louis, MO, USA; diluted 1:5000). The antigen-antibody complex was visualized with HRP-conjugated secondary antibody (Sigma, St. Louis, MO, USA; diluted 1:2000), and enhanced chemi luminescence detection reagent (Lilly, Indianapolis, IN, USA). The signal intensity was measured using an LAS-3000 imaging system (Fujifilm, Tokyo, Japan).

3.1.3 TEM images of cellular internalization studies

For internalization studies, U87MG and MCF7 cells were harvested and seeded into 24-well plates at 1×10^5 cells per well and incubated at 37°C overnight. To confirm receptor specific internalization of cRP-AuNPs, the cells were incubated with 0.3 mg/mL cRP-AuNPs for 30 min at 37°C in cultured media. Cells were then harvested and washed twice with phosphate buffered saline (PBS). The cells were fixed with 2% glutaraldehyde (GAA) for 1 day at 4°C, and they were deposited on a copper grid (300 mesh and covered with carbon). TEM images were then obtained by using JEOL (JEM-1400, JEOL, Tokyo, Japan) transmission electron microscope at an accelerating voltage of 80 keV. All the experiments were done in triplicate.

3.1.4 *In vitro* competitive cell binding assays

The IC_{50} value of cRGD, cRP-AuNPs (targeting nanoparticles), and mPEG-AuNPs (non-targeting nanoparticles, as control for comparison) were determined in U87MG and MCF7 cell lines. The cells were harvested and seeded into 24-well plates at 1×10^5 cells per well and incubated at 37°C overnight. The cells were then incubated with different concentrations of cRGD, cRP-AuNPs and mPEG-AuNPs (a serially diluted of concentrations of 0.1 pM to 100 μM were used) as blocking agents in cultured media, and ^{125}I-Echistatin (integrin $\alpha_v\beta_3$ specific) was also added. The concentration of ^{125}I-Echistatin added to the cells co-incubated with cRGD, cRP-AuNPs and mPEG-AuNPs was kept constant (7.4 kBq/well). The plate was then incubated for 30 min at 37°C, washed twice with phosphate buffered saline

(PBS), and then 0.5 mL of 0.5% SDS was added to each well to facilitate cell lysis. The lysates were collected and counted in a gamma counter (Packard, Meriden, CT). The cRGD concentration which reduces specific binding of ^{125}I-Echistatin by 50% (IC_{50}) was calculated by nonlinear regression analysis (sigmoidal dose response equation) using the GraphPad Prism 4.0 computer-fitting program (Graph-Pad Software, San Diego, CA, USA). All the experiments were repeated twice in triplicate.

3.1.5 CCK-8 cell proliferation assay

U87MG and MCF7 cell line were maintained in Minimum Essential Medium (MEM) and Dulbecco's Modified Eagle Medium (DMEM) supplemented with 10% FBS, penicillin, and streptomycin at 37^{o}C in a humidified atmosphere containing 5% CO_2. Individual wells of a 96-well microculture plate was filled with 5 × 10^3 cells/100 μL of cell suspension, and added with 0.005~0.5 mg/mL of cRP-AuNPs and 0.2% Triton X-100 as a positive control in a humidified incubator with 5% CO_2 for 24, 48 and 72 hrs at 37°C. The plate was treated with 10 μL/well of Cell Counting Kit-8 (CCK-8), and incubated in a CO_2 incubator for 2 hrs. The concentration that result in the inhibition of the cell growth was determined by assigning the mean value of the OD at 450 nm of the control wells on the third day as 100% after subtraction of the blank value. All the experiments were done in triplicate.

3.2 *In vivo* study

3.2.1 Tumor model and *in vivo* SPECT/CT imaging

All animal experiments were performed in compliance with the policies and procedures of Institutional Animal Care and Use Committee for animal treatment. In the right flank of 6-7 week-old BALB/c nude mice, 5×10^6 U87MG cells were implanted. Tumors were allowed to grow for 3 ~ 4 weeks after inoculation, at which time the animals received 11.1 MBq of ^{125}I-cRP-AuNPs and cRGD (10 mg/kg) blocked ^{125}I-cRP-AuNPs in 100 μL of PBS via lateral tail vein injection under isoflurane anesthesia. The images of the mice were taken using a small-animal imaging system with multi-pinhole collimation and a 15 to 45 keV photopeak energy window inside the SPECT/CT scanner (Bioscan, Washington DC, WA, USA). The SPECT images were obtained and performed at 32 projections over 360° (ROR=7.6 cm, 30 s/projection). The acquisition time depended on specific radioactivity levels in each mouse over the limits of the scan to obtain 100,000 c.p.s. SPECT scans were acquired at 10 min, 30 min, 1 hr, 3 hrs and 5 hrs after injection. Reconstructed data from SPECT and CT were visualized and co-registered using InVivoScope (Bioscan, Washington DC, WA, USA).

3.2.2 Biodistribution studies

BALB/c nude mice bearing U87MG xenografts were injected with ^{125}I-cRGD-AuNPs and cold form blocked ^{125}I-cRGD-AuNPs to evaluate the distribution of these tracers in the major organs of mice. The radiolabeled NPs

(~ 0.37 MBq) were injected via lateral tail vein. Mice (n = 3) were sacrificed at 1 hr post-injection (p.i.). Blood, tumor and major organs were removed and weighed. And radio-activity was measured in a gamma-counter (Packard, Meriden, CT, USA). The percent injected dose per gram (% ID/g) was then calculated.

3.2.3 TEM images of extracted organ tissues

For biopsy tumor tissue analysis, images of transmission electron microscopy (TEM) were taken using JEOL (JEM-1400, JEOL, Tokyo, Japan) transmission electron microscope at an accelerating voltage of 80 keV. For the preparation of extracted tumor tissues, 5×10^6 U87MG cells were implanted in the right flank of BALB/c nude mice. After allowing tumors to grow for 3 – 4 weeks, cRP-AuNPs (10 mg/kg) were injected intravenously via the mouse tail vein under isoflurane anesthesia. U87MG tumors, kidney, liver, lung, spleen were then extracted and fixed with 2% glutaraldehyde (GAA) for 7 days at 4°C, and they were deposited on a copper grid (300 mesh and covered with carbon). All the experiments were done in triplicate.

3.2.4 TEM images and radio TLC analysis of prepared urine samples

For collected urine sample analysis, images of transmission electron microscopy (TEM) were taken using JEOL (JEM-1400, JEOL, Tokyo, Japan) transmission electron microscope at an accelerating voltage of 80 keV. For the preparation of collected urine sample, ^{125}I-cRP-AuNPs (10 mg/kg) were

injected intravenously via the mouse tail vein under isoflurane anesthesia. After 1 hr urine samples were collected and fixed with 2% GAA solution. Radio TLC were analyzed of the urine samples from the ^{125}I-cRP-AuNPs i.v. injected mice (c), control free ^{125}I (d), control ^{125}I-cRGD-AuNPs (e).

3.2.5 *Ex vivo* organ tissue staining for fluorescence microscopy

Tumor and organ tissues produced from U87MG cells in BALB/c nude mice were removed and frozen at -80^{o}C. Frozen section slides (4 μm) of all the tissues were prepared after embedding in Tissue Tek® O.C.T. compound (Sakura Finetek, Torrance, CA, USA), which were fixed in acetone (-20°C, 20 min), incubated with 10% (v/v) FBS (room temperature, 30 min). And then stained with monoclonal $\alpha_v\beta_3$ antibody (MAB3050, R&D Systems, Minneapolis, MN, USA; diluted 1:100) at 4°C overnight, and then the slides were washed in PBS three times for 3 min. Then secondary anti-mouse IgG-PE antibody (562027, BD Pharmingen™, MA, USA) was applied and allowed to react for 2 hrs followed by washing in PBS three times for 3 min. For fluorescence microscopy, the stained tissues were mounted and counter-stained with DAPI mounting solution. Fluorescence was observed under an upright epifluorescence microscope (IX-71 Provis, Olympus, Rungis, France) equipped with a 100 W mercury vapor lamp and a Peltier cooled CCD camera

(DP71, Olympus, Rungis, France). All experiments were replicated at least three times for each animal on different days.

3.2.6 HQ silver enhancement staining for light microscopy

To visualize AuNPs located on tissue-section, we used HQ silver enhancement kit (Nanoprobes Inc. Stony Brook, NY, USA). Tumor and organ tissues produced from U87MG cells in BALB/c nude mice were removed and frozen at -80^{o}C. Frozen section slides (4 μm) of all the tissues were prepared after embedding in Tissue Tek® O.C.T. compound (Sakura Finetek, Torrance, CA, USA), which were fixed in acetone (-20°C, 20 min), incubated with 10% (v/v) FBS (room temperature, 30 min). Tissue sections were washed with 50 mM Tris buffer three times, distilled water three times, and 20 mM sodium citrate buffer. The initiator, moderator and activator included in the kit were mixed at a ratio of 1:1:1. The mixture was applied onto tissues and the intensity of staining was observed under microscope. The staining was stopped by washing with water three times for 10 min each. After washing with 100 mM phosphate buffer three times, the slides were viewed on a Leica DMLB microscope (Leica Microsystems, Wetzlar, Germany) and photographed. All experiments were replicated at least three times for each animal on different days.

RESULTS

1. Preparation of gold nanoparticles

1.1 Preparation and characterization of cRGD/Sulfo-SMCC/PEG-modified gold nanoparticles

In a typical experiment, 13 nm AuNPs were synthesized and modified with PEG (MW = 5 kD)-c(RGDyC) peptides for in vivo targeting of integrin $\alpha_v\beta_3$-positive tumor (Figure 1; please see the experimental section for details). Transmission electron microscopy (TEM) images showed cRGD-modified AuNPs were well dispersed with a narrow size distribution (Figure 2a). Considering that it showed neither solution color change nor UV-Vis spectral shift under various conditions (Figure 2c), I can conclude that the cRGD-conjugated AuNPs are highly stable under harsh conditions including high salt (1 M NaCl), strong acid (0.5 M HCl) and strong base (0.5 M NaOH) conditions (Figure 2b). The hydrodynamic diameter of the AuNPs with PEG-cRGD functional groups was measured by the dynamic light scattering (DLS) particle size analysis method (Zetasizer Nano, Malvern Instruments Ltd, England) and it was found to be ~31 nm (Figure 3b).

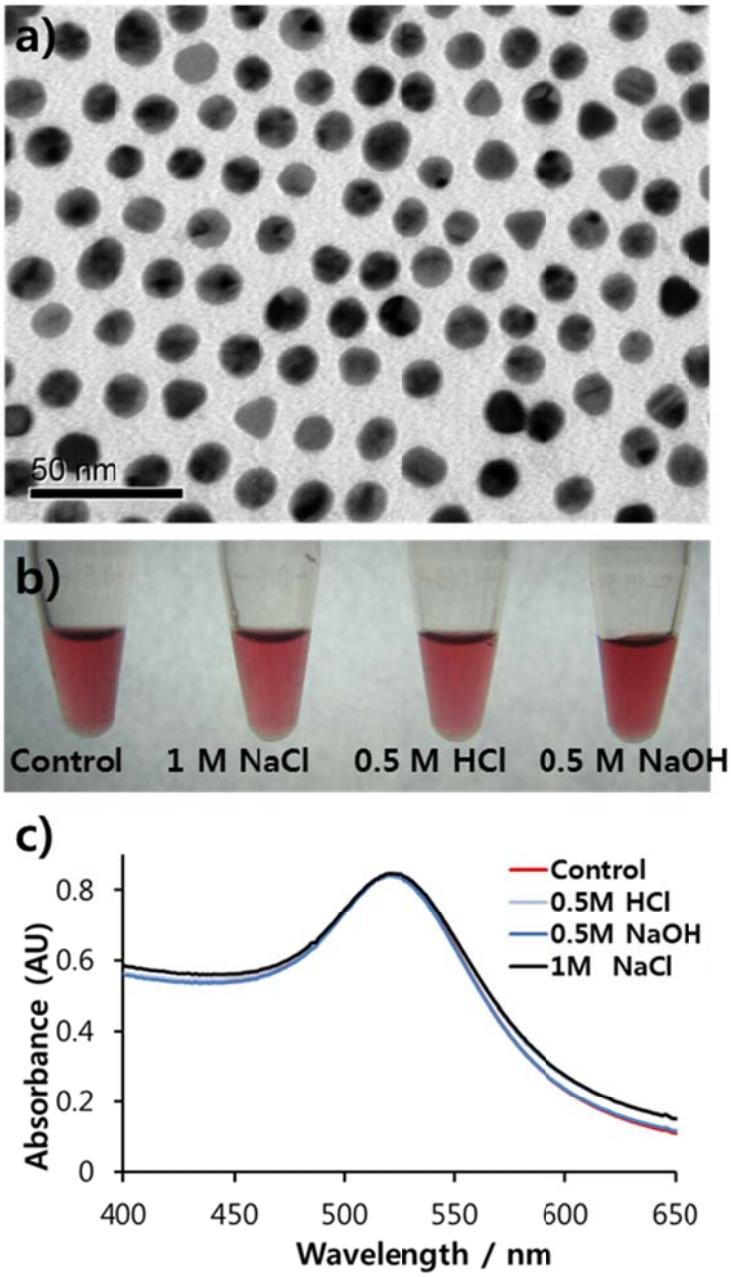

Figure 2. TEM image of cRP-AuNPs and stability test

(a) Transmission electron microscopy image of cRGD-PEG-modified AuNPs (cRP-AuNPs). Scale bar indicates 50 nm. (b, c) Stability test of ^{125}I-cRP-AuNPs in high salt, acidic and basic solutions (b) picture, (c) UV/Vis absorbance wavelength

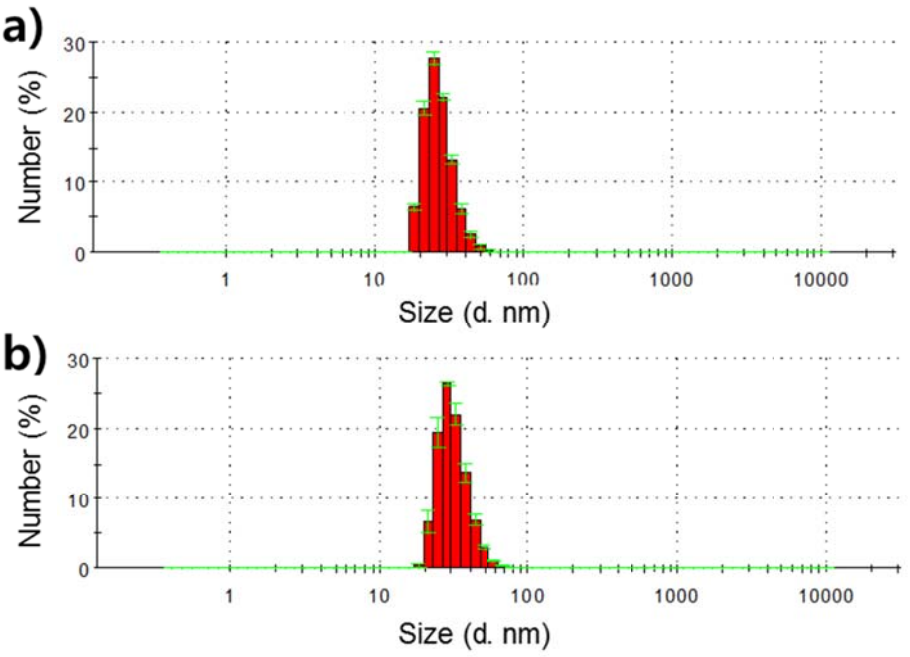

Figure 3. Size distributions mPEG-AuNPs and cRP-AuNPs

(a) Size distributions of mPEG-AuNPs measured by DLS The hydrodynamic size represents 26.87 ± 3.408 nm. (b) Size distributions of cRP-AuNPs measured by DLS. The hydrodynamic size represents 31.30 ± 4.052 nm. Data are expressed as means ± SDs of three independent experiments.

TABLE 1. Investigation of encapsulated AuNPs size, zeta-potential values, and polydispersity index determined by DLS

	mPEG-AuNPs	cRP-AuNPs
Size	26.87 ± 3.408 nm	31.30 ± 4.052 nm
Zeta-potential	-21.8 ± 0.728 mV	-26.3 ± 2.18 mV
Polydispersity index	0.461 ± 0.009	0.248 ± 0.017

The hydrodynamic size, zeta-potential values, and polydispersity index of encapsulated AuNPs before and after cRGD conjugation. Number average particle size was determined by DLS. Data are expressed as means ± SDs of three independent experiments.

1.2 Calculation of cRGD numbers per gold nanoparticles

The number of cRGDs on each AuNP whose surface was serially modified with amine-PEG-thiol, sulfo-SMCC and cRGDs, it was calculated by UV/Vis absorbance measurement. Control (cRGDyC) shows a λ_{max} peak at 275 nm. After the incubation with cRGDyC and centrifugation, supernatant from each eppendorf tube was collected separately. Then, UV/Vis absorption spectra of each supernatant were compared against cRGD solution of known concentration to quantify the number of cRGDs on each AuNP. The difference between UV/Vis aabsorbance of the cRGD in supernatant and pure cRGD (control) is 0.05764. Therefore, 33% of cRGD was conjugated to gold nanoparticles. My result shows that there are ~300 cRGD per particle (Figure 4). I also carried out experiments to show that there are no non-specific binding of cRGDs to AuNPs and that sulfo-SMCC are needed in order to conjugate cRGD peptides to PEGlylated AuNPs. The number of cRGDs on each AuNP whose surface is only modified with amine-PEG-thiol and cRGDs (i.e. no sulfo-SMCC) was calculated by the same method described in Figure 4. The data show that there are almost no non-specific binding of cRGD to AuNP surfaces (Figure 5).

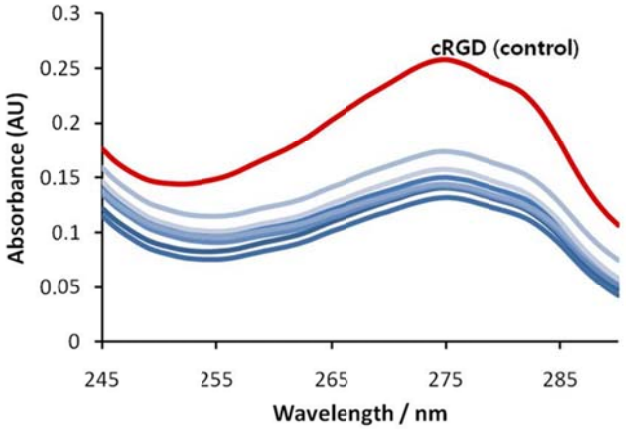

Name	Abs<275nm>
cRGD	0.17544
1	0.10967
2	0.10040
3	0.10931
4	0.10832
5	0.12277
6	0.10677
7	0.11178
8	0.10780
9	0.11536
10	0.10337
Average	0.11780

Figure 4. Calculation of the number of cRGDs on each AuNP

The number of cRGDs on each AuNP whose surface is serially modified with amine-PEG-thiol, sulfo-SMCC and cRGDs, it was calculated by UV/Vis absorbance measurement. Control (cRGDyC) shows a λ_{max} peak at 275 nm. After the incubation with cRGDyC and centrifugation, supernatant from each eppendorf tube was collected separately. Then, UV/Vis absorption spectra of each supernatant were compared against cRGD solution of known concentration to quantify the number of cRGDs on each AuNP. The difference between UV/Vis absorbance of the cRGD in supernatant and pure cRGD (control) is 0.05764. Therefore, 33% of cRGD was conjugated to gold nanoparticles. That is ~300 cRGD molecules per AuNP.

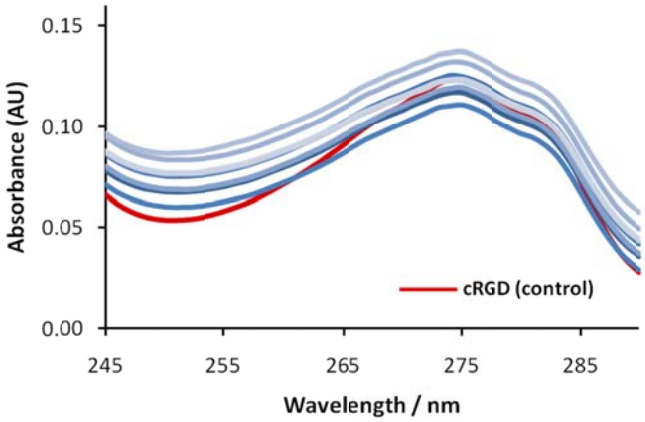

Name	Abs<275nm>
cRGD	0.1239
1	0.1448
2	0.1247
3	0.1251
4	0.1245
5	0.111
6	0.1196
7	0.1192
8	0.1373
9	0.123
10	0.1237
Average	0.1253

Figure 5. Calculation of the number of nonspecific cRGDs on each AuNP

The number of cRGDs on each AuNP whose surface is only modified with amine-PEG-thiol and cRGDs (i.e. no sulfo-SMCC) was calculated by the same method described in Figure 4. The data show that there are almost no non-specific binding of cRGD to AuNP surfaces.

1.3 cRGD-PEGylated gold nanoparticles with ^{125}I radiolabeling

For quantitative *in vitro* and *in vivo* study, the iodine-labeled cRGD-PEG-AuNPs (^{125}I-cRP-AuNPs) were purified by centrifugation (12000 rpm for 15 min), the labeling efficiency was determined by measuring gamma-radiation emission from the gold pellet and supernatant, respectively. For radioactive iodine labeling to cRGD-PEG-AuNPs, 10 μCi/10 μL of [^{125}I]NaI in PBS solution was added to 100 μL cRP-AuNPs solution (7 nM), and the resulting solution was stirred for 5 min at ambient temperature. The radiochemical yield of the procedure was higher than 99% (Figure 6a). Radio labeling efficiencies were analyzed by thin layer chromatography. For this analysis, ITLC-SG was eluted with saline solution (pH 7.4); free ^{125}I moved with front line (R_f=1.0) and ^{125}I-cRP-AuNPs remained at the origin (R_f=0.0). The labeling efficiency was higher than 99.15 ± 1.35% (n=3), and free ^{125}I was not found after purification. By taking into account of the specific activity (17 Ci/mg) and half-life (60.14 days) of ^{125}I, we can calculate the number of moles of ^{125}I (4.21×10^{-12} moles). Since the number of moles of AuNP probes is 7.0×10^{-13} moles, it is calculated to give that there are ~6 radioactive iodine-125 isotopes conjugated per cRP-AuNP probe. For the confirmation of ^{125}I labeling on the AuNP surface, ^{125}I-cRP-AuNP pellet was treated with 1.5 M dithiothreitol (DTT) solution. After 1 hr incubation, AuNPs were aggregated via ligand exchange with DTT, and >90% of ^{125}I was liberated from AuNPs (Figure 6a). These results proved that ^{125}I forms bonds to the AuNP surfaces when [^{125}I]NaI solution was mixed with the AuNP solution. Further, the stability of these probes was extensively tested in various pH

conditions, and the results show that these probes are very stable from pH 2-8 at room temperature for 24 hrs (Figure 6b). Finally, serum stability test results showed that more than 85% of ^{125}I was remained intact on AuNPs after 24 hrs incubation at 37^{o}C (Figure 6c). Non-targeted mPEG-AuNPs, to which cRGD was not modified, also displayed similar radio-labeling efficiency and serum stability (Figure 6c).

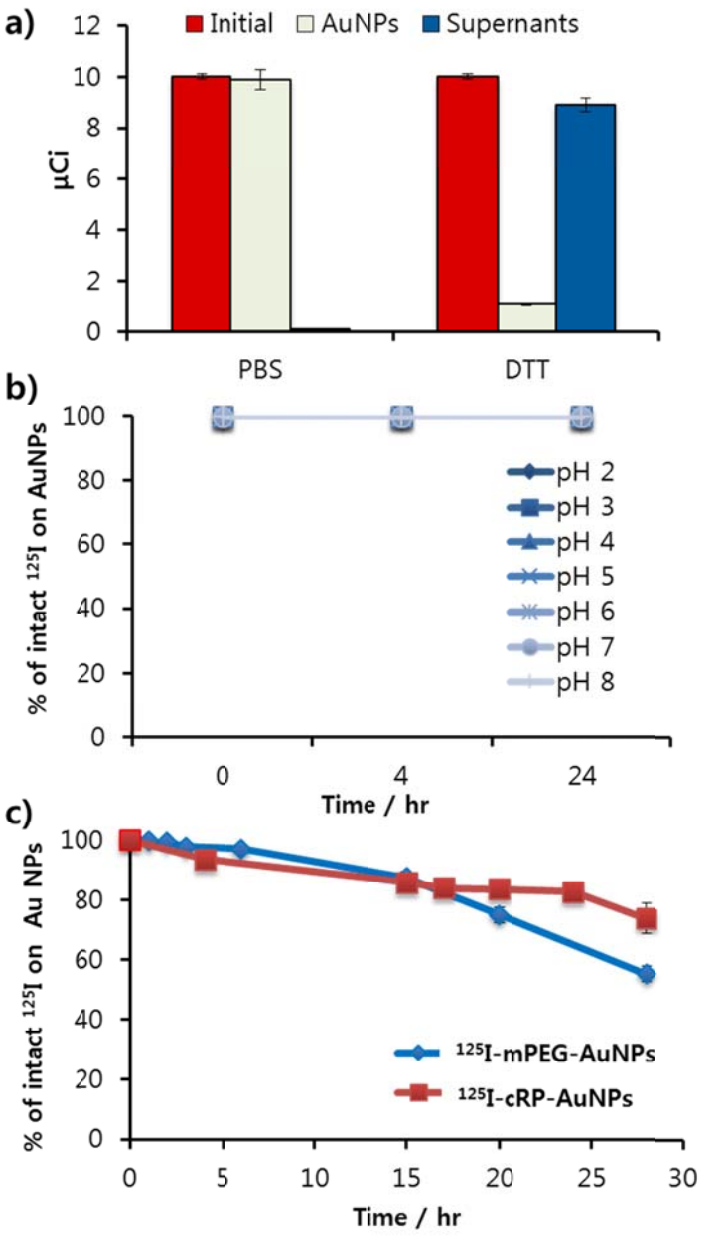

Figure 6. Efficiency and labeling stability of ^{125}I labeling with cRP-AuNPs
(a) Efficient ^{125}I labeling on AuNPs in PBS solution. ^{125}I was liberated in DTT solution (b, c) Stability tests of ^{125}I-cRP-AuNPs and ^{125}I-mPEG-AuNPs over 24 hrs incubation in different pH conditions (b) and serum (c) conditions

2. *In vitro* study of cRGD conjugated AuNPs target to integrin $\alpha_v\beta_3$

To evaluate the ^{125}I-cRP-AuNP as an imaging probe for integrin $\alpha_v\beta_3$-positive tumor, I tested their targeting ability with U87MG (high integrin $\alpha_v\beta_3$ expression) and MCF7 (integrin $\alpha_v\beta_3$ negative) cell lines.

2.1 Integrin $\alpha_v\beta_3$ expression of cells

I confirmed the mRNA and protein expression levels of α_v and β_3 in U87MG and MCF7 cells using the reverse-transcriptase polymerase chain reaction (RT-PCR) and western blot (Figure 7 a, b). The PCR data indicate that the 319-bp and 301-bp fragments were detected from the expression of α_v mRNA and β_3 mRNA in U87MG cells while no α_v or β_3 mRNA fragments were found from MCF7 cells (Figure 7a). According to the protein expression results, 113 kDa of $\alpha_v\beta_3$ protein clearly appeared in only U87MG cells, not in MCF7 cells (Figure 7b).

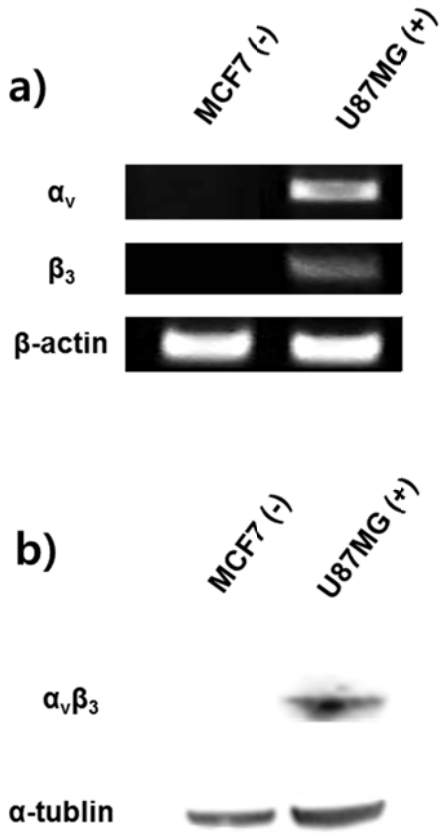

Figure 7. Confirmation the expression of integrin $\alpha_v\beta_3$

(a) RT-PCR analysis. Expression of α_v and β_3 in U87MG, MCF7 cells were determined by RT-PCR. The 319-bp fragments were detected the expression of α_v mRNA, and 301-bp fragments were detected the expression of β_3 mRNA in U87MG cells. β-actin was used as an internal loading control.

(b) Western blot analysis. Expression of $\alpha_v\beta_3$ in U87MG, MCF7 cells was determined by western blot. 113 kDa were detected in U87MG cells. α-tublin was used as an internal loading control.

2.2 CCK-8 proliferation assay

To evaluate the cytotoxicity of the ^{125}I-cRP-AuNPs, I assessed cell proliferation by CCK-8 assay (Figure 8). The assay results proved that the ^{125}I-cRP-AuNP probes are not cytotoxic even with a high probe concentration and a prolonged incubation time for both U87MG and MCF7 cell lines (Figure 8 a,b). These probes were completely cell-viable even after incubation with the loading of ^{125}I-cRP-AuNP probes (0.5 mg/mL) per 5 $\times$ 10^3 cells for up to 72 hrs.

2.3 TEM images of integrin $\alpha_v\beta_3$ receptor-mediated endocytosis

To confirm receptor-specific internalization of the AuNPs, I investigated cellular uptake of the probes by U87MG and MCF7 cells by the sectional TEM technique after co-incubating each cell line with ^{125}I-cRP-AuNPs separately (please see the experimental section for the experimental details). The ^{125}I-cRP-AuNPs were localized in the intracellular regions of $\alpha_v\beta_3$-positive U87MG cells (Figure 9a). On the other hand, only negligible amount of particles were found inside $\alpha_v\beta_3$-negative MCF7 cells (Figure 9b). The results demonstrate that the ^{125}I-cRP-AuNPs entered the cells via integrin $\alpha_v\beta_3$-receptor-mediated endocytosis.

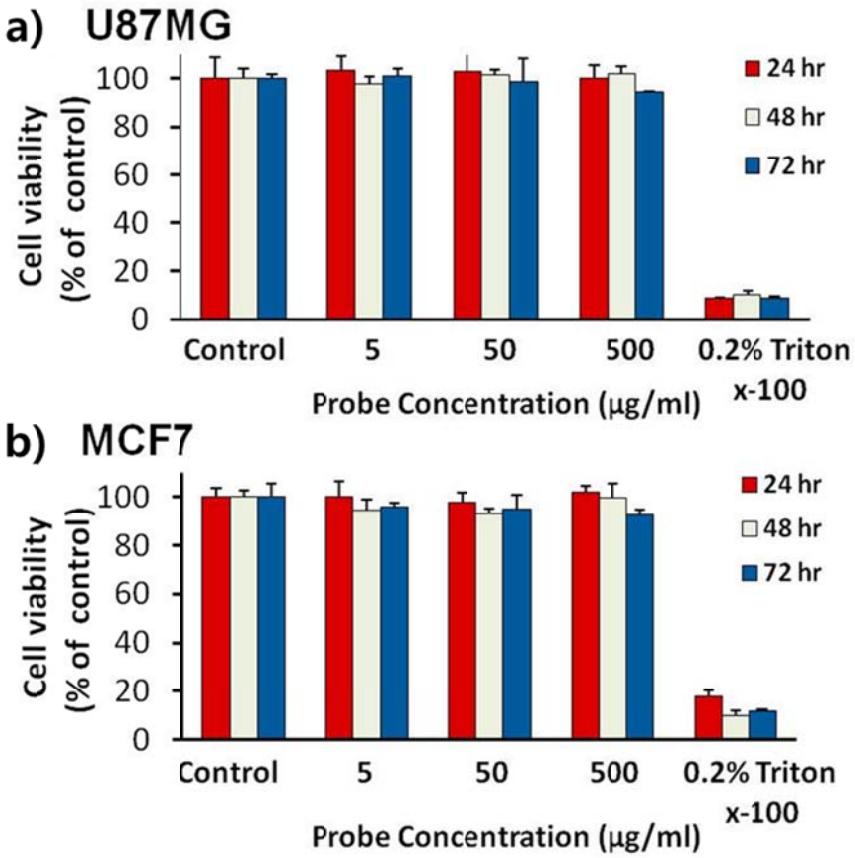

Figure 8. **Cell proliferation assay**

(a,b) CCK-8 proliferation assay: (a) U87MG and (b) MCF7 cells were treated with different amounts of ^{125}I-cRP-AuNPs and 0.2% Triton X-100 as a positive control and incubated for 24, 48 and 72 hours. The results are presented as percentage absorbance relative to control cells incubated in probe-free medium. Data are expressed as means ± SDs of three independent experiments.

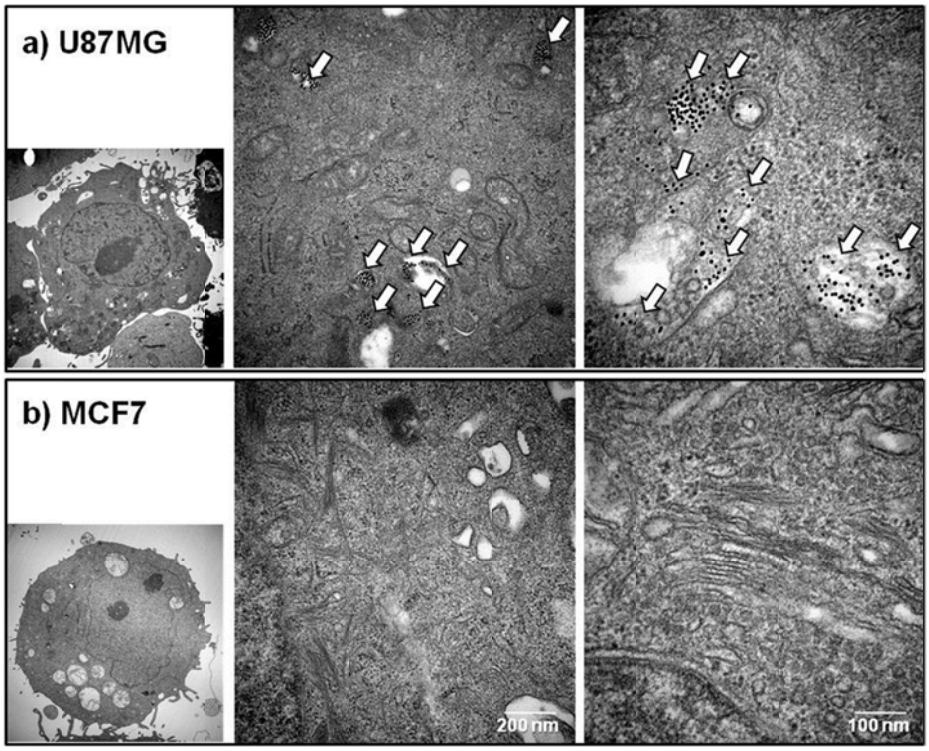

Figure 9. TEM images of cellular uptake

(a, b) TEM images of cellular uptake after treated with cRP-AuNPs. U87MG cells (a) and MCF-7 cells (b) were incubated with cRP-AuNPs (300 μg/ml) for 30 min. Arrows indicate cellular uptake of cRP-AuNPs. U87MG cells (a) only show strong uptake of cRP-AuNPs in cells. Scale bar indicates 100, 200 nm

2.4 Integrin $\alpha_v\beta_3$ competitive cell binding assay

Next, to investigate the integrin-binding affinity and specificity of the AuNPs, competitive binding assays were carried out using ^{125}I-echistatin as the $\alpha_v\beta_3$ integrin-specific radioligand (*36*), (*46*). The serially diluted, cRGD peptides, mPEG-AuNPs, and the cRP-AuNPs (0.1 pM to 100 μM) were added as integrin blocking agents to cells in a culture medium, respectively. For U87MG cells, as the concentration of integrin blocking agents (for both cRGD peptides and cRP-AuNPs) increased, the percent of cell-bound ^{125}I-echistatin was significantly decreased. This means that cRGD peptides and cRP-AuNPs inhibited the binding of ^{125}I-echistatin to $\alpha_v\beta_3$ integrins. Importantly, the IC_{50} values for cRGD and cRP-AuNPs were 51.34 ± 2.0 and 0.337 ± 0.16 nmol/L, respectively. The cell-binding assay results also demonstrate that cRP-AuNPs has ~150-fold higher $\alpha_v\beta_3$ integrin avidity than the corresponding cRGD peptide analogs. The mPEG-AuNPs did not inhibit the binding of ^{125}I-echistatin to the U87MG cells, and this shows the mPEG-AuNPs without cRGD functionality do not affect the receptor avidity of the cells. In the case of MCF7 cell line, even with an increase in the amount of cRGD peptides, ^{125}I-cRP-AuNPs, or mPEG-AuNPs, the percent of bound ^{125}I-echistatin was not affected or affected only negligibly. The results clearly show that the cRGD peptides and ^{125}I-cRP-AuNPs specifically inhibited the binding of ^{125}I-echistatin to $\alpha_v\beta_3$ integrin-positive U87MG cells, but they did not inhibit the binding of ^{125}I-echistatin to $\alpha_v\beta_3$ integrin-negative MCF7 cells was observed (Figure 10).

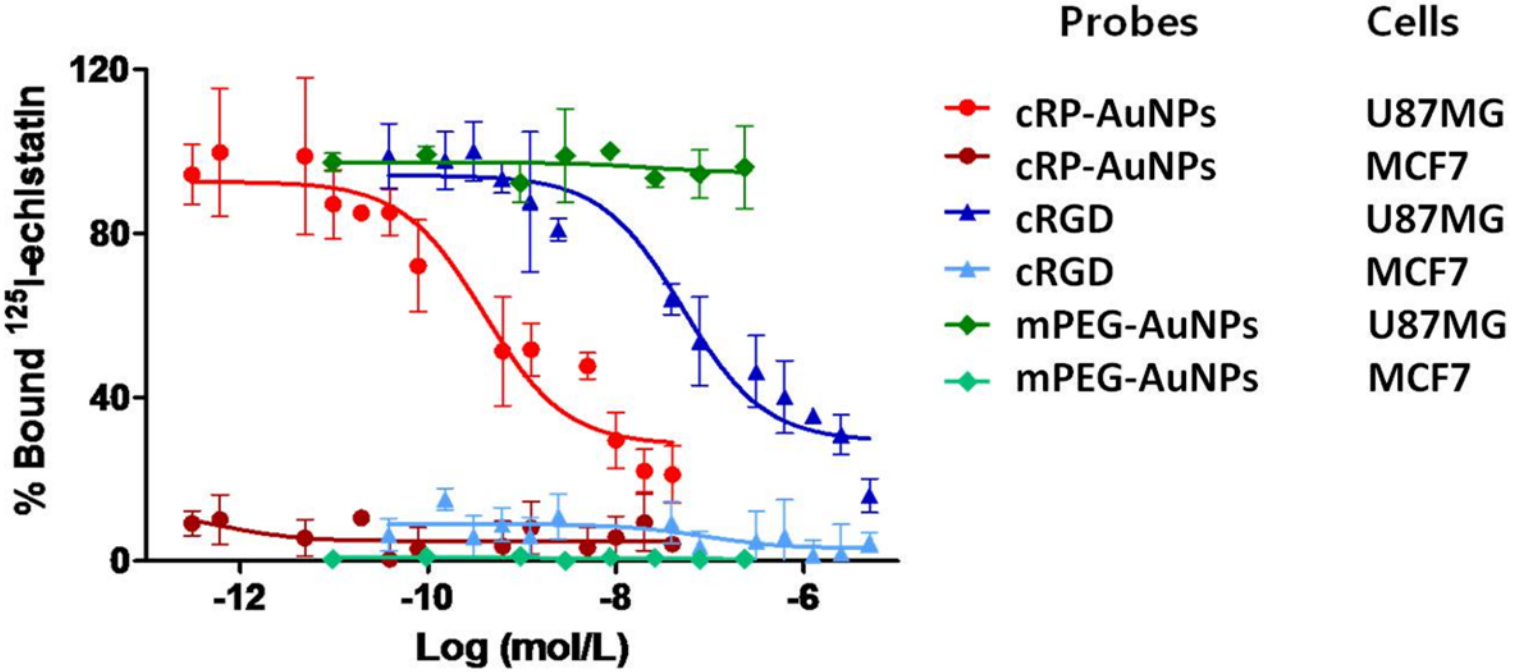

Figure 10. Competitive binding assay

Inhibition of ^{125}I-echistatin (integrin $\alpha_v\beta_3$-specific) binding to $\alpha_v\beta_3$ integrin on U87MG and MCF cells by cRGD peptide, mPEG-AuNPs, and cRGD-PEG-AuNPs (n = 3, mean ± SD), respectively. The IC_{50} values for the cRGD peptide and cRGD-PEG-AuNPs are 51.34 and 0.337 nM, respectively. Experiment was repeated twice in triplicate.

3. *In vivo* study of cRGD conjugated AuNPs target to integrin $\alpha_v\beta_3$

3.1 *In vivo* SPECT/CT image of tumor angiogenesis

Finally, the usefulness of ^{125}I-cRP-AuNPs as *in vivo* imaging probes was tested and evaluated with the SPECT/CT technique. ^{125}I-cRP-AuNPs and cold-form blocked ^{125}I-cRP-AuNPs (10 mg/kg for each) were injected intravenously via a mouse tail vein. For cold-form blocking studies, unlabeled cRP-AuNPs (50 mg/kg) and ^{125}I-cRP-AuNPs (10 mg/kg) were co-injected to tumor bearing mouse. Their biodistribution and tumor targeting from in a nude mouse were imaged and analyzed (Figure 11). The SPECT/CT results show that the ^{125}I-cRP-AuNPs targeted tumor site quickly and effectively within 10 min after injection (Figure 11a). Remarkably, it appears that probes were gradually further deposited at tumor site as time elapsed while overall probe signals got weaker at the sites other than tumor region, instead probes were accumulated in the bladder. In the case of cold-form blocked ^{125}I-cRP-AuNPs, tumor was almost undetectable and imaging signals were much stronger in non-tumor parts of body (Figure 11b). The difference in imaging signal intensity in tumor site between targeting and cold-form blocked ^{125}I-cRP-AuNP probes gets wider and clearer as more time elapses.

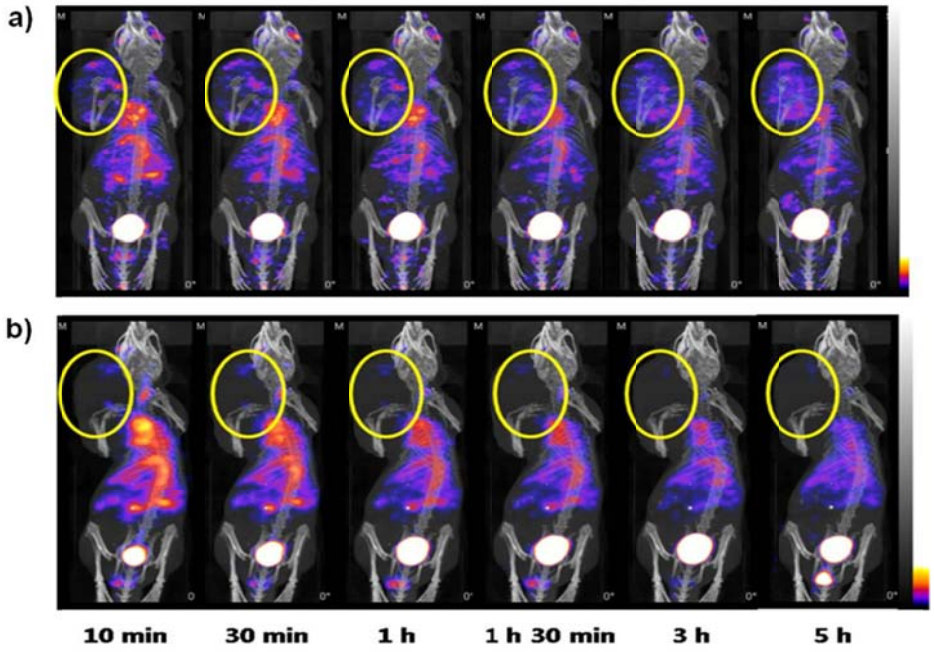

Figure 11. ***In vivo*** **small-animal SPECT/CT images**

(a) Small-animal SPECT/CT images of ^{125}I-cRP-AuNPs, and (b) cold form blocked ^{125}I-cRGD-AuNPs in a nude mice bearing U87MG tumors xenografts after injection through tail vein. The SPECT/CT studies were performed serially from 0 hr to 5 hrs after injection of 11.1 MBq radiolabeled Au-NPs. Yellow circle indicates tumor region.

3.2 Biodistribution study

Using ^{125}I-cRP-AuNPs, and cold form blocked ^{125}I-cRP-AuNPs, we followed distribution in all organs and blood 1 hr after intravenous injection. 1 hr after intravenous injection of ^{125}I-cRP-AuNPs, the appreciable distribution was highly blood activity (6.0 ± 1.4% injected dose/gram; %ID/g) and tumor (4.9 ± 1.7% injected dose/gram; %ID/g), with the latter likely representing ^{125}I-cRGD-AuNPs in the process of being excreted (Figure. 12). In contrast, uptakes in tumor %ID/g values for cold form blocked ^{125}I-cRGD-AuNPs exhibited 2.2 ± 0.1%ID/g (Figure. 12).

3.3 *Ex vivo* urine sample analysis

After 1 hr of ^{125}I-cRP-AuNPs injection, we have collected urine samples from the mice to analyze the excretion of the probes. TEM images of the collected urine samples confirm the renal filtration of cRP-AuNPs (Figure 13a). We have also carried out and radio-TLC analysis of the urine sample (Figure 13b). For this analysis, ITLC-SG was eluted with saline solution (pH 7.4); free ^{125}I moved with front line (R_f=1.0) and ^{125}I-cRP-AuNPs remained at the origin (R_f=0.0). The results show that 59.1% of ^{125}I is attached to gold nanoparticle surfaces (figure 13b).

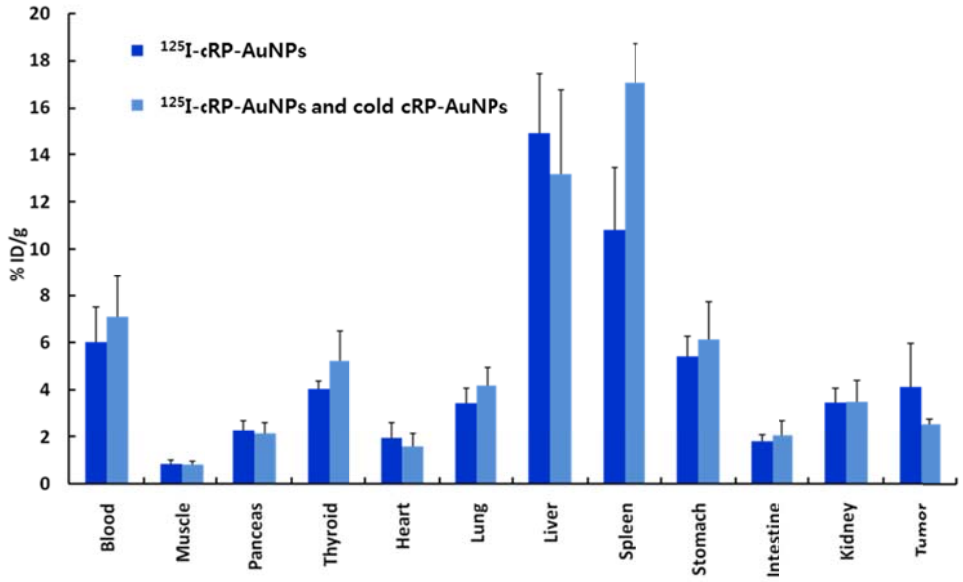

Figure 12. Biodistribution

BALB/c nude mice bearing U87MG xenografts were injected with ^{125}I-cRP-AuNPs and cold form blocked ^{125}I-cRP-AuNPs through tail vein. Biodistribution studies were performed at 1 hr after injection of 0.37 MBq radiolabeled Au-NPs. The percent injected dose per gram (% ID/g) was then calculated. (n=3)

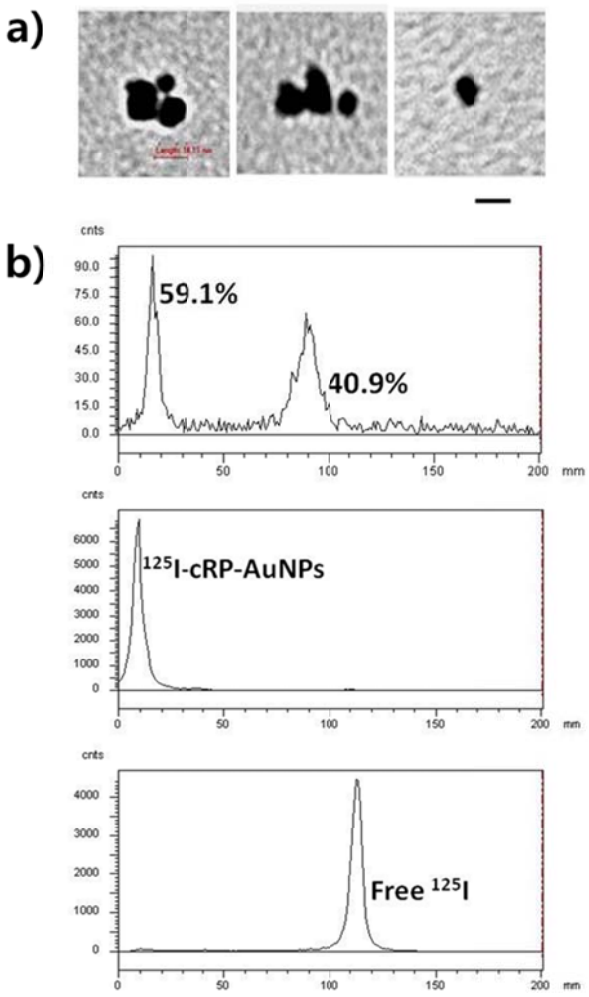

Figure 13. Analysis of collected urine sample

(a) TEM images of gold nanoparticles obtained from urine samples. Data obtained from tumor 1 hr after injection. (b) Radio TLC analysis of urine sample of mice treated with ^{125}I-cRP-AuNPs (200 μg/mouse). 59.1% of the ^{125}I collected 1 hr after the injection is bound to gold nanoparticles.

3.4 *Ex vivo* TEM images of tumor and organ

The extracted tumor tissues were analyzed by TEM imaging technique to confirm the uptake of ^{125}I-cRP-AuNPs by the tumor and various organs (figure 14, 15). The images clearly show the ^{125}I-cRP-AuNPs are uptake by the tumor (figure 14). These results demonstrate that the ^{125}I-cRP-AuNPs entered the tumor via integrin $\alpha_v\beta_3$-receptor specific endocytosis.

3.5 *Ex vivo* integrin $\alpha_v\beta_3$ and gold nanoparticle staining of tumor and organ tissue

To confirm specific integrin $\alpha_v\beta_3$ binding and secretion properties of these particles, I examined the extracted tumor and organ tissue. After 1 hr of ^{125}I-cRP-AuNPs injection, the tumor tissue was well correlated with $\alpha_v\beta_3$-PE (figure 16a), DAB (figure 16b) staining regions and Au silver enhancement staining regions (figure 16c). These results demonstrate that high affinity of RGD ligand to $\alpha_v\beta_3$ integrin could be applicable for angiogenesis imaging in tumor model. The various organs (muscle, kidney, liver, spleen and lung) also were observed (figure 17). The result showed the muscle region (figure 17a) was not observed $\alpha_v\beta_3$ and Au silver enhancement staining. Kidney (figure 17b), liver (figure 17c), lung (figure 17e) regions were well correlated with $\alpha_v\beta_3$-PE staining region and Au silver enhancement staining areas. But spleen (figure 17d) region was not stained $\alpha_v\beta_3$, but stained with

Au silver enhancement only. The result showed that the spleen organ was not expressed integrin $\alpha_v\beta_3$, but just removed ^{125}I-cRP-AuNPs from organism and moderated by macrophages. This demonstrates that the ^{125}I-cRP-AuNPs secreted via kidney, liver, and spleen.

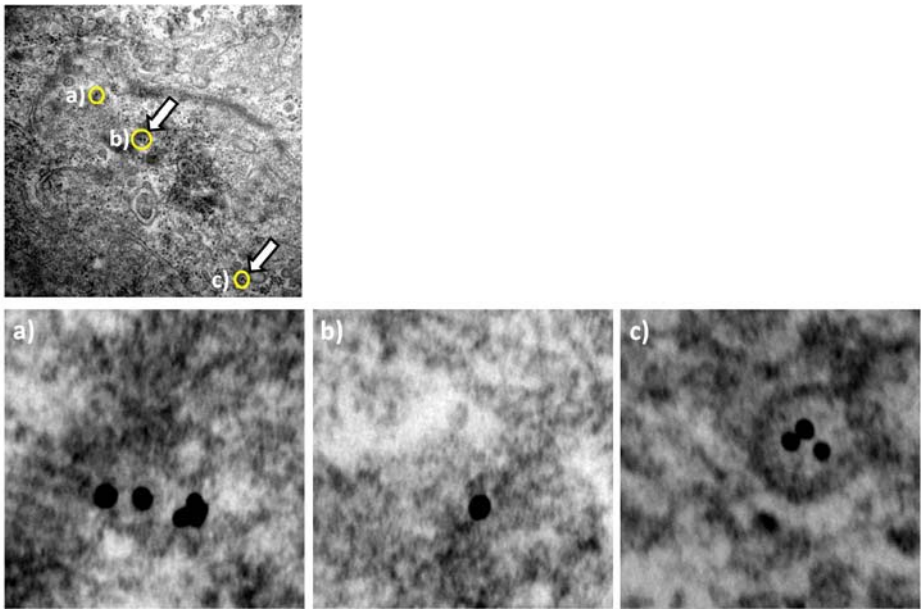

Figure 14. Biopsy tumor tissue was analyzed under TEM

The images clearly show the ^{125}I-cRP-AuNPs are uptake by the tumor. This demonstrates that the ^{125}I-cRP-AuNPs entered the tumor via integrin $\alpha_v\beta_3$-receptor specific endocytosis.

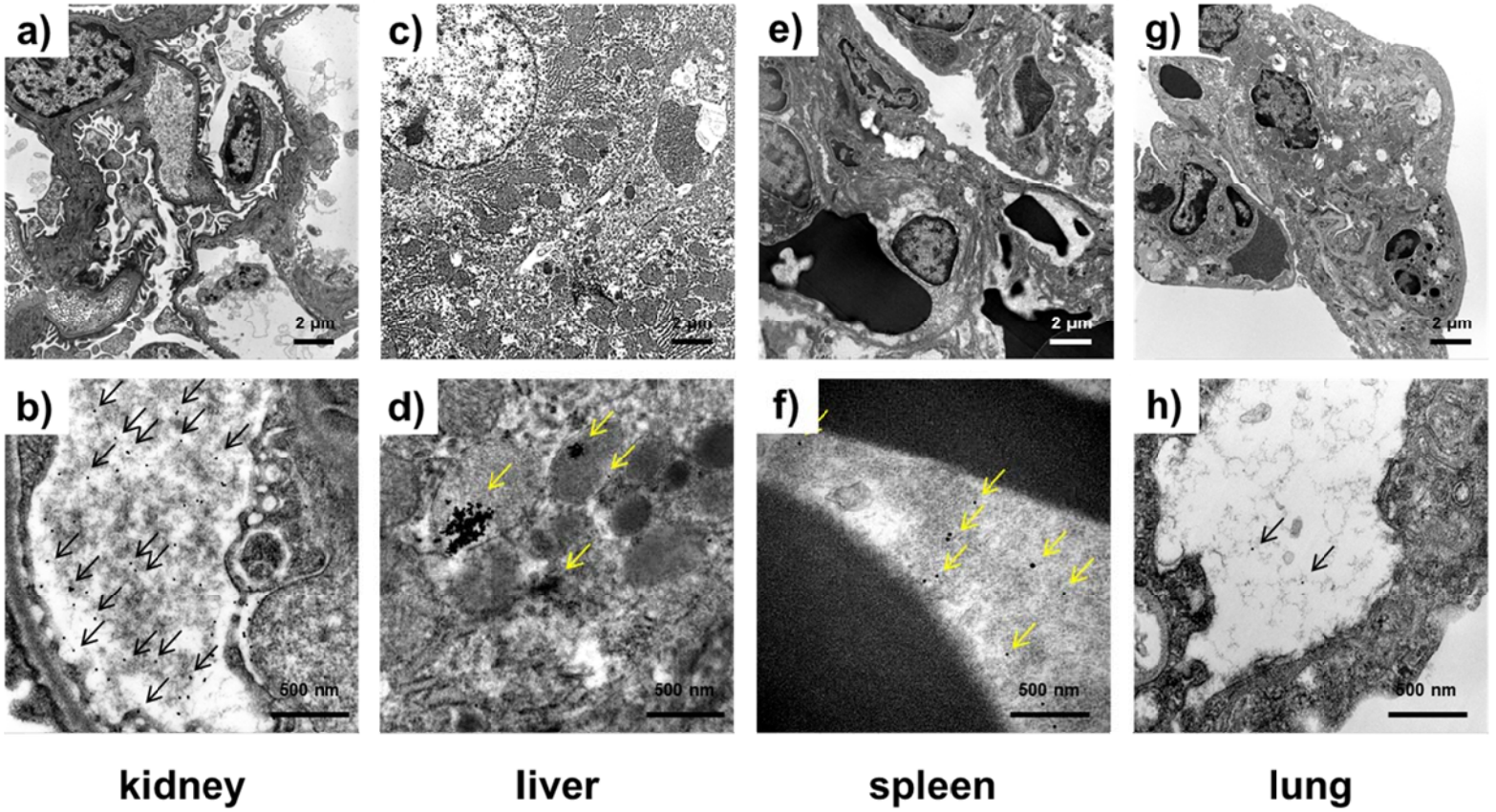
a)
c)
e)
g)
2 µm
2 µm
2 µm
2 µm
b)
d)
f)
h)
500 nm
500 nm
500 nm
500 nm
kidney
liver
spleen
lung

Figure 15. Extracted organ tissue was analyzed under TEM

Kidney (a, b), liver (c, d), spleen (e, f), lung (g, h) were specifically observed ^{125}I-cRP-AuNPs. This demonstrates that the ^{125}I-cRP-AuNPs secreted via kidney, liver, and spleen. TEM image was monitored by low-power field (a, c, e, f) and. (b, d, f, h) high power field (the black dot indicates gold nanoparticle.)

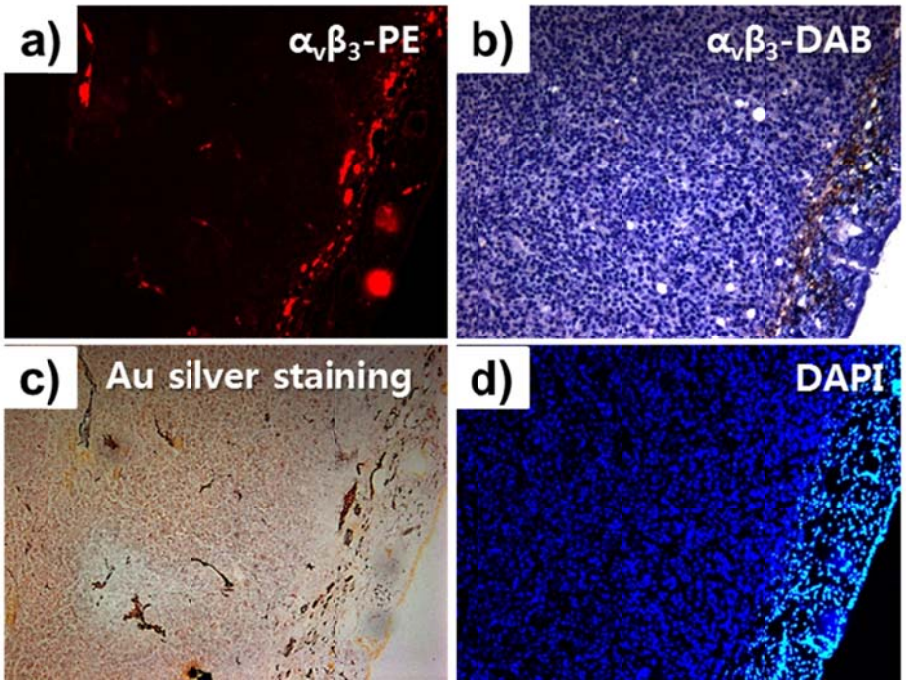

Figure 16. Histopathology of extracted tumor tissue

Extracted tumor tissue was stained with $\alpha_v\beta_3$ and Au silver enhancement. The tumor tissue was well correlated with $\alpha_v\beta_3$ PE (a), DAB (b) staining region and Au silver enhancement staining areas. This demonstrates that the ^{125}I-cRP-AuNPs specifically targeted the tumor via integrin $\alpha_v\beta_3$-receptor specific endocytosis. ($\alpha_v\beta_3$-PE: red, DAPI: blue, Au-silver enhancement: pink)

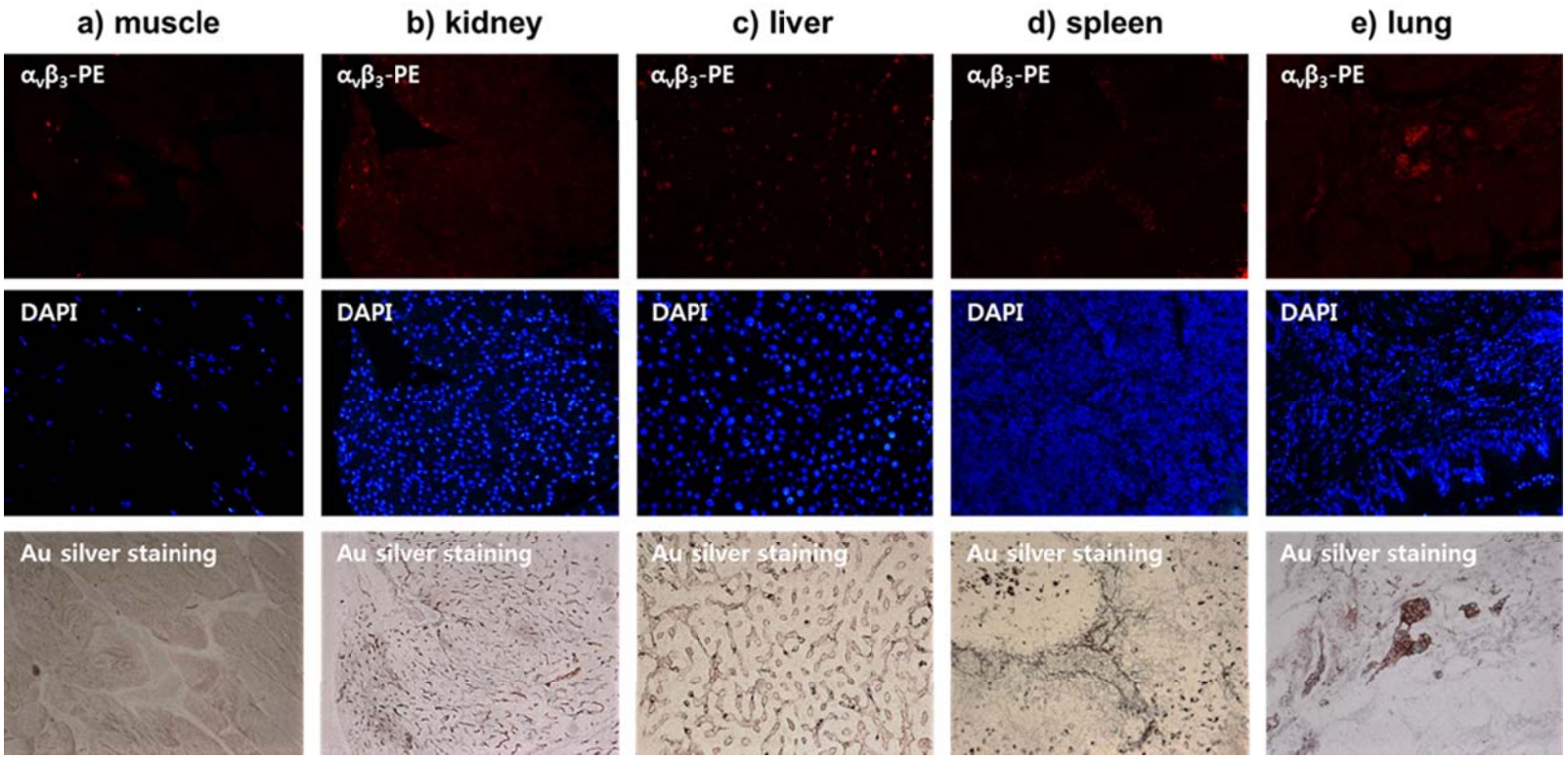
a) muscle
b) kidney
c) liver
d) spleen
e) lung
αvβ3-PE
DAPI
Au silver staining

Figure 17. Histopathology of extracted organ tissue

The extracted organ tissue was stained with $\alpha_v\beta_3$ and Au silver enhancement. Muscle region (a) was not observed $\alpha_v\beta_3$ and Au silver enhancement staining. Kidney (b), liver (c), lung (e) regions were well correlated with $\alpha_v\beta_3$-PE staining region and Au silver enhancement staining areas. And spleen (d) region was not stained $\alpha_v\beta_3$, but stained with Au silver enhancement only. This demonstrates that the ^{125}I-cRP-AuNPs secreted via kidney, liver, and spleen. ($\alpha_v\beta_3$-PE: red, DAPI: blue, Au-silver enhancement: pink)

DISCUSSION

Nanotechnology is emerging for important new applications of nanomaterials in various fields (*23*). Various nanomaterials are attractive due to their own charming points. These multifunction nanomaterials can be used for diagnostic *in vitro* and *in vivo* and therapeutic purpose as well. For example there are novel drug delivery, biological imaging, and cancer treatment systems such as liposomes, micelles, gold nanoparticles, and silica nanoparticles at different stages of pre-clinical and clinical development (*10*).

Aim of this study was to evaluate ^{125}I-labeled gold nanoparticles (AuNPs) conjugated with PEG-RGD peptides for targeting tumor. Imaging modality was SPECT/CT and gold nanoparticles were used as a platform for labeling of the radioactive iodine as well as conjugation of targeting groups, PEG-RGD peptides.

Angiogenesis imaging may turn out to have significant benefits because they evaluate other diseases characterized by abnormal angiogenesis, such as ischemic region and benign tumors. Already many research groups have shown the various radio-labeled RGD sequence targeted imaging method in biomedical area (*43-45*). However, a small peptide that consists of the radio-labeled RGD sequence is quickly the washing out *in vivo* (*44*). And also their targeting affinity is reduced to compare RGD peptide conjugated nanoparticles because nanoparticles can load several hundreds of peptide on their large surface. In my experimental condition, cRP-AuNPs has a $\alpha_v\beta_3$

integrin avidity more than 150 times compare to the cRGD peptide (Figure 10). In the analysis of extracted tumor tissue, integrin $\alpha_v\beta_3$ and Au silver stained tissue were well correlated. This demonstrates that the ^{125}I-cRP-AuNPs specifically targeted the tumor via integrin $\alpha_v\beta_3$-receptor-specific endocytosis (Figure 16). However, integrin $\alpha_v\beta_3$ and Au silver stained regions were concentrated in angiogenesis vessel regions, because integrin $\alpha_v\beta_3$ expression level of tumor angiogenesis regions were much higher than integrin $\alpha_v\beta_3$-positive tumor.

There are several reports that endocytosis might make cells to uptake nanomaterials, by mainly target to the macropinocytosis, clathrin-mediated, caveolin-mediated, and clathrin/caveolin-independent endocytosis machinery (*47,48*). It also was reported that endocytosis could be affected by surface chemistiry modified nanomaterials. Various nanomaterials with poly(ethylene) glycol (PEG), a surface chemistry commonly used to prevent nonspecific protein binding, was found to prevent this aggregation (*49*). However, it was reported that long PEG chain can reduce specific binding of ligand as well as non-specific binding (*50*). In this study, PEG^{5000} was suitable, because it could significantly reduce non-specific binding effectively and did not block the specific binding of RGD ligand. Moreover, I extensively showed the ^{125}I-cRP-AuNPs works out well for tumor-targeted imaging applications in *in vitro* and *in vivo* condition (Figure 9, 11).

Despite the PEGylation of AuNPs, targeting efficiency to tumor site was lower than to the liver and spleen. The efficiency of various kinds of nanoparticles, such as gold nanoparticles to target the tumor remains to be elucidated. Further studies are needed to reduce the non-specific liver and spleen uptakes in *in vivo* condition.

It is critical to note the use of the non-degradable nanoparticles, which is currently focused on excretion from the body, before the proof of targeting can be determined. Frangioni et al. have demonstrated the requirements for renal filtration and urinary excretion of inorganic, metal-containing nanoparticles using quantum dots. In this case the material was not applied for in vivo imaging yet and also they reported that the hydrodynamic diameter by >15 nm prevented renal excretion. (*51*) It was previously known that only the nanoparticles with sizes less than 5.5 nm can be excreted through renal filtration. However, there are several journals published recently which demonstrate that nanoparticles with sizes bigger than 5 - 6 nm go through renal filtration. It can actually be excreted depending on their shapes and surface chemistry (*52-54*). Biological tissues and cells are all soft materials and, although the hydrodynamic radius of our particles is ~ 31 nm, the hard core size of my probes is only ~ 13 nm. After 1 hr of ^{125}I-cRP-AuNPs injection, I have collected urine samples from the mice to analyze the excretion of the probes. TEM images of the collected urine samples confirm the renal filtration of cRP-AuNPs (Figure 13a). I have also carried out radio-TLC analysis of the urine sample. The results show that 59.1% of ^{125}I is

attached to gold nanoparticle surfaces (Figure 13b). So, I persist my probes can be squeezed by other structures and go through soft renal filtration structures.

Despite of the gold nanoparticles are well known inert to the body and not lethal to the cells, it may affect intracellular responses and potential mechanisms in biological systems (*27*,*30*). Therefore, considerable effort is needed to validate the potential risks of nanoparticles to cells and organisms. Due to their large surface area per unit mass and high catalytic activity, these nanoparticles have strong tendency to agglomerate in biological fluids (*55*). That means these nanoparticles interact with biomolecules such as proteins and DNA in biological environment. More and accurate results are needed for biological specific mechanism by gold nanoparticles; further studies are necessary to test how to respond the cells that could be affected either directly or indirectly by gold nanoparticles.

In summary, I developed that cyclic RGD-PEGylated-AuNPs was labeled with ^{125}I (^{125}I-cRP-AuNPs) as molecular imaging probes. The conjugated probes were stable for ~20 hrs in serum or under various pH and high salt conditions. Importantly, I showed ^{125}I-cRP-AuNPs specifically targeted to tumor cells and the probes were taken up by tumor cells via integrin $\alpha_v\beta_3$-receptor-mediated endocytosis with almost no cytotoxicity. The ^{125}I-cRP-AuNPs have ~150-fold higher $\alpha_v\beta_3$ integrin avidity than non-modified free cRGD peptides. Finally, *in vivo* SPECT/CT imaging results

proved that the ^{125}I-cRP-AuNPs can target tumor and angiogenesis sites only after 10 min from intravenous injection. These promising results demonstrate that radioactive ^{125}I and RGD-PEG functionalized AuNPs can be used as targeted tumor SPECT/CT imaging and angiogenesis-targeted imaging probes, which will be useful for various diagnostic and therapeutic applications.

REFERENCES

1. Weissleder R, Pittet MJ. Imaging in the era of molecular oncology. *Nature.* Apr 3 2008;452(7187):580-589.

2. Czernin J, Allen-Auerbach M, Schelbert HR. Improvements in cancer staging with PET/CT: literature-based evidence as of September 2006. *J Nucl Med.* Jan 2007;48 Suppl 1:78S-88S.

3. Messiou C, Orton M, Ang JE, et al. Advanced solid tumors treated with cediranib: comparison of dynamic contrast-enhanced MR imaging and CT as markers of vascular activity. *Radiology.* Nov 2012;265(2):426-436.

4. Jones T, Price P. Development and experimental medicine applications of PET in oncology: a historical perspective. *The lancet oncology.* Mar 2012;13(3):e116-125.

5. Massoud TF, Gambhir SS. Molecular imaging in living subjects: seeing fundamental biological processes in a new light. *Genes Dev.* Mar 1 2003;17(5):545-580.

6. Wang LV, Hu S. Photoacoustic tomography: in vivo imaging from organelles to organs. *Science.* Mar 23 2012;335(6075):1458-1462.

7. Meng Q, Li Z. Molecular imaging probes for diagnosis and therapy evaluation of breast cancer. *Int J Biomed Imaging.* 2013;2013:230487.

8. Goodwin R, Giaccone G, Calvert H, Lobbezoo M, Eisenhauer EA. Targeted agents: how to select the winners in preclinical and early clinical studies? *Eur J Cancer.* Jan 2012;48(2):170-178.

9. Harney AS, Meade TJ. Molecular imaging of in vivo gene expression. *Future Med Chem.* Mar 2010;2(3):503-519.

10. Jaffer FA, Weissleder R. Molecular imaging in the clinical arena. *JAMA.* Feb 16 2005;293(7):855-862.

11. Weissleder R, Ntziachristos V. Shedding light onto live molecular targets. *Nat Med.* Jan 2003;9(1):123-128.

12. Troyan SL, Kianzad V, Gibbs-Strauss SL, et al. The FLARE intraoperative near-infrared fluorescence imaging system: a first-in-human clinical trial in breast cancer sentinel lymph node mapping. *Ann Surg Oncol.* Oct 2009;16(10):2943-2952.

13. Agdeppa ED, Spilker ME. A review of imaging agent development. *AAPS J.* Jun 2009;11(2):286-299.

14. Monopoli MP, Aberg C, Salvati A, Dawson KA. Biomolecular coronas provide the biological identity of nanosized materials. *Nat Nanotechnol.* Dec 2012;7(12):779-786.

15. Alkilany AM, Lohse SE, Murphy CJ. The Gold Standard: Gold Nanoparticle Libraries To Understand the Nano-Bio Interface. *Acc Chem Res.* Jun 25 2012.

16. Chen H, Li B, Wang C, et al. Characterization of a fluorescence probe based on gold nanoclusters for cell and animal imaging. *Nanotechnology.* Feb 8 2013;24(5):055704.

17. Cheon J, Lee JH. Synergistically integrated nanoparticles as multimodal probes for nanobiotechnology. *Acc Chem Res.* Dec 2008;41(12):1630-1640.

18. Giljohann DA, Mirkin CA. Drivers of biodiagnostic development. *Nature.* Nov 26 2009;462(7272):461-464.

19. Goesmann H, Feldmann C. Nanoparticulate functional materials. *Angew Chem Int Ed Engl.* Feb 15 2010;49(8):1362-1395.

20. Kang B, Mackey MA, El-Sayed MA. Nuclear targeting of gold nanoparticles in cancer cells induces DNA damage, causing cytokinesis arrest and apoptosis. *J Am Chem Soc.* Feb 10 2010;132(5):1517-1519.

21. Lee S, Xie J, Chen X. Peptides and peptide hormones for molecular imaging and disease diagnosis. *Chem Rev.* May 12 2010;110(5):3087-3111.

22. Wang J, Tian S, Petros RA, Napier ME, Desimone JM. The complex role of multivalency in nanoparticles targeting the transferrin receptor for cancer therapies. *J Am Chem Soc.* Aug 18 2010;132(32):11306-11313.

23. Xia Y. Nanomaterials at work in biomedical research. *Nat Mater.* Oct 2008;7(10):758-760.

24. Hong S, Leroueil PR, Majoros IJ, Orr BG, Baker JR, Jr., Banaszak Holl MM. The binding avidity of a nanoparticle-based multivalent targeted drug delivery platform. *Chem Biol.* Jan 2007;14(1):107-115.

25. Maus L, Dick O, Bading H, Spatz JP, Fiammengo R. Conjugation of peptides to the passivation shell of gold nanoparticles for targeting of cell-surface receptors. *ACS Nano.* Nov 23 2010;4(11):6617-6628.

26. Montet X, Montet-Abou K, Reynolds F, Weissleder R, Josephson L. Nanoparticle imaging of integrins on tumor cells. *Neoplasia.* Mar 2006;8(3):214-222.

27. Alkilany AM, Murphy CJ. Toxicity and cellular uptake of gold nanoparticles: what we have learned so far? *J Nanopart Res.* Sep 2010;12(7):2313-2333.

28. Cobley CM, Chen J, Cho EC, Wang LV, Xia Y. Gold nanostructures: a class of multifunctional materials for biomedical applications. *Chem Soc Rev.* Jan 2011;40(1):44-56.

29. Hainfeld JF, Slatkin DN, Focella TM, Smilowitz HM. Gold nanoparticles: a new X-ray contrast agent. *Br J Radiol.* Mar 2006;79(939):248-253.

30. Murphy CJ, Gole AM, Stone JW, et al. Gold nanoparticles in biology: beyond toxicity to cellular imaging. *Accounts of chemical research.* Dec 2008;41(12):1721-1730.

31. Rhim WK, Kim JS, Nam JM. Lipid-gold-nanoparticle hybrid-based gene delivery. *Small.* Oct 2008;4(10):1651-1655.

32. Brandenberger C, Muhlfeld C, Ali Z, et al. Quantitative evaluation of cellular uptake and trafficking of plain and polyethylene glycol-coated gold nanoparticles. *Small.* Aug 2 2010;6(15):1669-1678.

33. Cai W, Shin DW, Chen K, et al. Peptide-labeled near-infrared quantum dots for imaging tumor vasculature in living subjects. *Nano Lett.* Apr 2006;6(4):669-676.

34. Eck W, Craig G, Sigdel A, et al. PEGylated gold nanoparticles conjugated to monoclonal F19 antibodies as targeted labeling agents for human pancreatic carcinoma tissue. *ACS Nano.* Nov 25 2008;2(11):2263-2272.

35. Lipka J, Semmler-Behnke M, Sperling RA, et al. Biodistribution of PEG-modified gold nanoparticles following intratracheal instillation and intravenous injection. *Biomaterials.* Sep 2010;31(25):6574-6581.

36. Alric C, Taleb J, Le Duc G, et al. Gadolinium chelate coated gold nanoparticles as contrast agents for both X-ray computed tomography and magnetic resonance imaging. *J Am Chem Soc.* May 7 2008;130(18):5908-5915.

37. Marradi M, Alcantara D, de la Fuente JM, Garcia-Martin ML, Cerdan S, Penades S. Paramagnetic Gd-based gold glyconanoparticles as

probes for MRI: tuning relaxivities with sugars. *Chem Commun (Camb).* Jul 14 2009(26):3922-3924.

38. Kim D, Park S, Lee JH, Jeong YY, Jon S. Antibiofouling polymer-coated gold nanoparticles as a contrast agent for in vivo X-ray computed tomography imaging. *J Am Chem Soc.* Jun 20 2007;129(24):7661-7665.

39. Cheng W, Dong S, Wang E. Iodine-induced gold-nanoparticle fusion/fragmentation/aggregation and iodine-linked nanostructured assemblies on a glass substrate. *Angew Chem Int Ed Engl.* Jan 27 2003;42(4):449-452.

40. Hong H, Zhang Y, Sun J, Cai W. Molecular imaging and therapy of cancer with radiolabeled nanoparticles. *Nano Today.* Oct 1 2009;4(5):399-413.

41. Shao X, Agarwal A, Rajian JR, Kotov NA, Wang X. Synthesis and bioevaluation of (1)(2)(5)I-labeled gold nanorods. *Nanotechnology.* Apr 1 2011;22(13):135102.

42. Chen X, Park R, Shahinian AH, Bading JR, Conti PS. Pharmacokinetics and tumor retention of 125I-labeled RGD peptide are improved by PEGylation. *Nucl Med Biol.* Jan 2004;31(1):11-19.

43. Cai W, Chen X. Preparation of peptide-conjugated quantum dots for tumor vasculature-targeted imaging. *Nat Protoc.* 2008;3(1):89-96.

44. Jeong JM, Hong MK, Chang YS, et al. Preparation of a promising angiogenesis PET imaging agent: 68Ga-labeled c(RGDyK)-isothiocyanatobenzyl-1,4,7-triazacyclononane-1,4,7-triacetic acid and feasibility studies in mice. *J Nucl Med.* May 2008;49(5):830-836.

45. Wu Y, Zhang X, Xiong Z, et al. microPET imaging of glioma integrin {alpha}v{beta}3 expression using (64)Cu-labeled tetrameric RGD peptide. *J Nucl Med.* Oct 2005;46(10):1707-1718.

46. Alford R, Ogawa M, Choyke PL, Kobayashi H. Molecular probes for the in vivo imaging of cancer. *Mol Biosyst.* Nov 2009;5(11):1279-1291.

47. Blander JM, Medzhitov R. On regulation of phagosome maturation and antigen presentation. *Nat Immunol.* Oct 2006;7(10):1029-1035.

48. Aderem A, Underhill DM. Mechanisms of phagocytosis in macrophages. *Annu Rev Immunol.* 1999;17:593-623.

49. Eghtedari M, Liopo AV, Copland JA, Oraevsky AA, Motamedi M. Engineering of hetero-functional gold nanorods for the in vivo molecular targeting of breast cancer cells. *Nano Lett.* Jan 2009;9(1):287-291.

50. Kirpotin D, Park JW, Hong K, et al. Sterically stabilized Anti-HER2 immunoliposomes: Design and targeting to human breast cancer cells in vitro. *Biochemistry-Us.* Jan 7 1997;36(1):66-75.

51. Choi HS, Liu W, Misra P, et al. Renal clearance of quantum dots. *Nat Biotechnol.* Oct 2007;25(10):1165-1170.

52. Lacerda L, Herrero MA, Venner K, Bianco A, Prato M, Kostarelos K. Carbon-nanotube shape and individualization critical for renal excretion. *Small.* Aug 2008;4(8):1130-1132.

53. Cho M, Cho WS, Choi M, et al. The impact of size on tissue distribution and elimination by single intravenous injection of silica nanoparticles. *Toxicol Lett.* Sep 28 2009;189(3):177-183.

54. Caliceti P, Veronese FM. Pharmacokinetic and biodistribution properties of poly(ethylene glycol)-protein conjugates. *Adv Drug Deliv Rev.* Sep 26 2003;55(10):1261-1277.

55. Chatterjee S, Bandyopadhyay A, Sarkar K. Effect of iron oxide and gold nanoparticles on bacterial growth leading towards biological application. *J Nanobiotechnology.* 2011;9:34.

국문 초록

서론: 생리학 분야에서 분자 영상 및 약물 전달 등에 생체 친화적인 나노 입자를 사용할 수 있다. 이 연구에서는 생체 내에서 종양의 신생혈관을 영상화 하기 위해서, 인테그린 $\alpha_v\beta_3$ 를 표적 하는 RGD 와 방사성 옥소-125 가 표지된 금 나노 입자를 개발하였다.

재료 및 방법: 금 나노입자에 인테그린 $\alpha_v\beta_3$ 를 세포주를 표적 하는 RGD 를 결합하고, 생체 적합성을 높이기 위한 PEG 가 결합된 금나노 입자 (^{125}I-cRP-AuNP)를 합성하였다. 방사성 옥소-125 를 표지한 후, 표지 효율을 확인하였고, 16 시간 동안 37°C 의 혈청 내 상태에서의 표지 효율의 안정성을 관찰하였다. RGD 를 결합한 금 나노 입자 (cRP-AuNP)가 인테그린 $\alpha_v\beta_3$ 에 특이적으로 결합하는지 확인하기 위해, U87MG (인테그린 $\alpha_v\beta_3$ 과발현), MCF-7 (인테그린 $\alpha_v\beta_3$ 비 발현) 세포주를 이용하여 cRGD 와 cRP-AuNPs 를 세포에 미리 처리한 후, ^{125}I-echistatin 방사성 물질을 이용한 경쟁적 결합 분석을 시행하였다. 방사성 옥소-125 의 세포 내 섭취는 감마카운터를 사용하여 측정하였다. cRP-AuNPs 의 수용체 특이적 세포내 섭취의 여부를 확인하기 위하여, U87MG (인테그린 $\alpha_v\beta_3$ 과 발현), MCF-7 (인테그린 $\alpha_v\beta_3$ 비 발현) 세포주에 300 μg/mL 의 cRP-AuNPs 처리 후, 전자 현미경으로 관찰하였다. U87MG 세포를 이종 이식한 쥐 모델에서

방사성 옥소-125 를 표지한 ^{125}I-cRP-AuNsP 과 cRP-AuNPs (100 mg/kg)이 포함된 ^{125}I-cRP-AuNPs 를 각각 정맥 투여 후 0 ~ 5 시간 동안 단일 광자 방사 단층 촬영 영상을 획득하였다. 금 나노 입자가 인테그린 $\alpha_v\beta_3$ 에 특이적으로 표적됨을 확인하기 위하여, 정맥주사 후 적출된 종양 조직에서 전자현미경 영상 및 인테그린 $\alpha_v\beta_3$ 면역 염색을 시행하였다. 또한 ^{125}I-cRP-AuNP 의 생체 내 신장배출을 확인하기 위하여, 소변 샘플에서의 방사능-TLC 분석하였다.

결과: RGD 를 도입한 금 나노 입자에 방사성 옥소-125 를 표지한 ^{125}I-cRP-AuNP 의 전체 과정은 20 분 이내로 완료되었다. ^{125}I-cRP-AuNP 의 표지 효율은 100%이고, 37°C 의 혈청 내 상태에서의 표지 효율의 안정성은 3 시간에는 97%, 16 시간째는 88%로 안정하였다. U87MG (인테그린 $\alpha_v\beta_3$ 과 발현) 세포주에서 경쟁적 결합력을 분석한 결과, cRP-AuNPs 및 cRGD 의 펩티드에 대한 IC_{50} 값은 각각 0.33 nM 와 51.34 nM 이었다. cRP−AuNP 입자는 cRGD 펩티드 보다 150 배 높은 인테그린 $\alpha_v\beta_3$ 친화도를 확인하였다. cRP-AuNP 처리 후, 전자 현미경으로 관찰한 영상에서는 인테그린 $\alpha_v\beta_3$ 과 발현 세포주 U87MG 세포주에서만 특이적으로 관찰되었다. U87MG 세포를 이종이식한 쥐 모델에서 ^{125}I-cRP-AuNPs 를 정맥 주사한 후 촬영한 단일 광자 방사 단층 영상에서, 주사 후 10 분 이후부터 종양 특이적인 영상 및 혈관 조영이 관찰되었다. 정맥 주사한 후 적출된 종양 조직의 전자현미경 영상에서 금 나노 입자가 관찰되었으며, 인테그린

$\alpha_v\beta_3$ 면역 염색에서도 염색부위와 금 나노 입자의 분포 부위가 일치하였다. 또한 신장과 비뇨기 배설 경로를 통해 생체 내에서 배출되는 것을 확인하였다. 소변 샘플의 방사능-TLC 분석을 통하여 방사성 옥소-125 를 표지한 ^{125}I-cRP-AuNPs 물질이 소변을 통해 50% 이상 관찰되는 것을 확인 하였다.

결론: ^{125}I-cRP-AuNPs 이 실험관 내와 마우스 실험에서 모두 인테그린 $\alpha_v\beta_3$ 발현 암 세포 및 신생혈관을 특이적으로 표적 할 수 있었다. 이러한 기능적인 ^{125}I-cRP-AuNPs 을 활용하면 종양 및 혈관 신생을 표적 하는 다양한 진단 및 치료에 유용 할 것으로 기대된다.

주요어: 금 나노입자, 나노입자의 독성, 종양 신생혈관 표적, 종양 신생혈관 영상, 인테그린 $\alpha_v\beta_3$, 방사성 옥소-125, 단일 광자 방사 단층촬영법

학 번: 2008-23291